INTEGRATED RADIO FREQUENCY LC VOLTAGE-CONTROLLED OSCILLATORS

by

Joo Leong Tham

Memorandum No. UCB/ERL M95/33

22 May 1995

INTEGRATED RADIO FREQUENCY LC VOLTAGE-CONTROLLED OSCILLATORS

by

Joo Leong Tham

Memorandum No. UCB/ERL M95/33

22 May 1995

ELECTRONICS RESEARCH LABORATORY

College of Engineering
University of California, Berkeley
94720

Integrated Radio Frequency LC Voltage-Controlled Oscillators

Joo Leong Tham

May, 1995

Abstract

A monolithic radio frequency fully differential LC voltage-controlled oscillator using on-chip spiral inductors and varactors has been designed and fabricated. Measured results of the VCO are presented. A non-intrusive empirical method of determining oscillator output to resonator isolation is presented. Resonator topologies have been investigated for reliable start-ups with findings of an additional start-up criteria for harmonic oscillators. Approaches to minimize phase noise were investigated.

Table of Contents

1 Introduction

Voltage-controlled oscillators (VCOs) circuits are widely used in communication systems for modulation and demodulation of signals. Fig. 1.1 shows the basic elements of a communication system. With the anticipated growth in microwave communication systems such as the Global Positioning System (GPS), Direct Broadcast Satellite (DBS), Personal Communication Networks (PCN), and mobile radio, there is an increasing need for giga-hertz range VCO's with high output spectral purity. Good phase noise performance is important in narrow-band applications for minimizing the system noise contribution of the VCOs; phase noise performance is one of the limiting factors that determine the minimum (frequency domain) spacing between two communication channels.

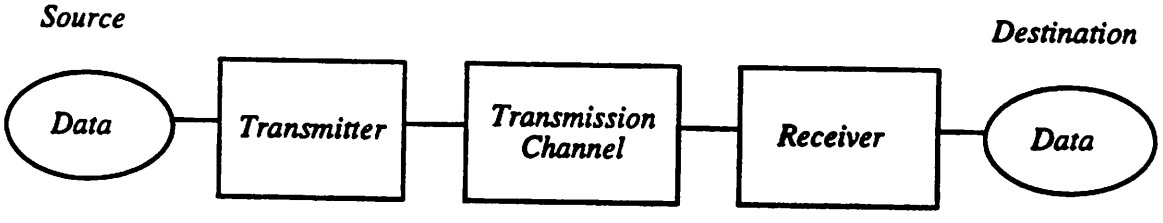

Fig. 1.1 Elements of a Communication System

VCOs are commonly configured as a block, in frequency synthesizers, to provide frequency references for mixers to perform frequency translation. The frequency synthesizer is fed with a high stability frequency reference such as a crystal-controlled oscillator (XCO) and to produce a programmable output frequency proportional to the reference. It may optionally be configured to provide multiple referenced outputs for signal processing. A VCO is shown in Fig. 1.2 in a portable transceiver architecture as an illustration of one of its applications.

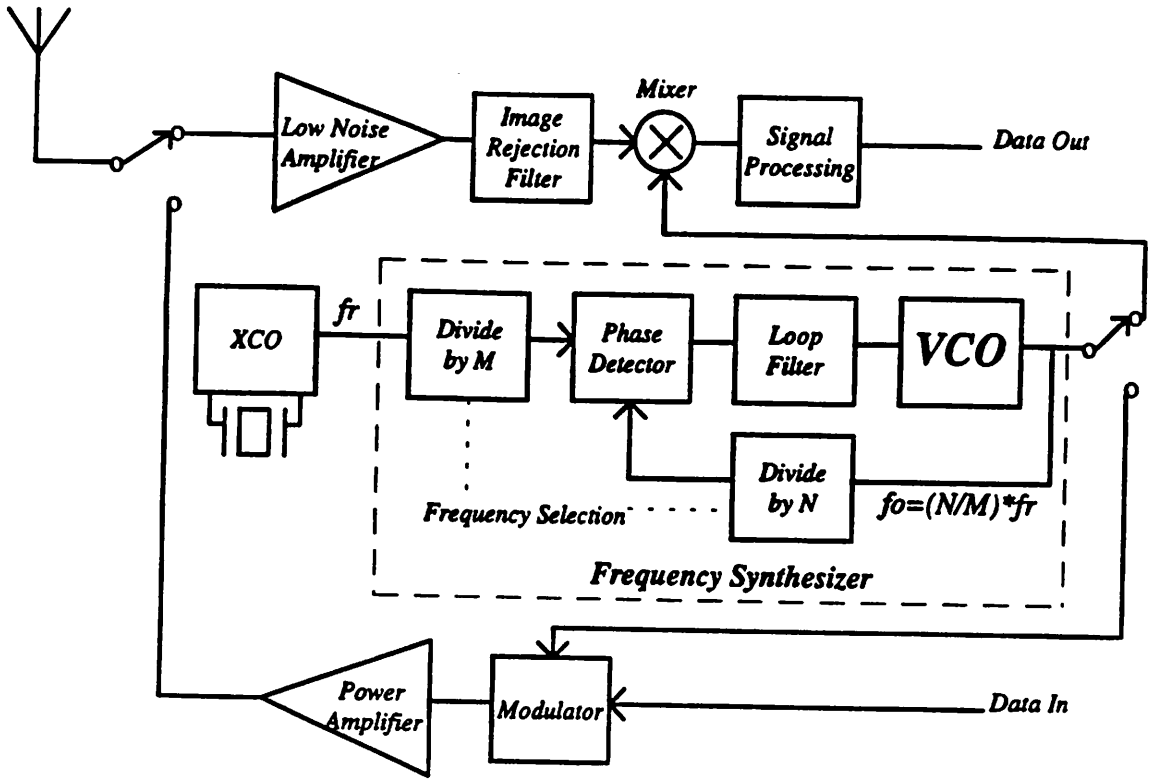

Fig. 1.2 Portable Transceiver Architechure

Voltage-controlled oscillators are used as FM modulators as well. They are also frequently used in phaselocked loops (PLL) where demodulation of modulated signals or recovery of clock signals are performed. Fig 1.3 shows a PLL with pick-off points for recovery of three different types of modulation.

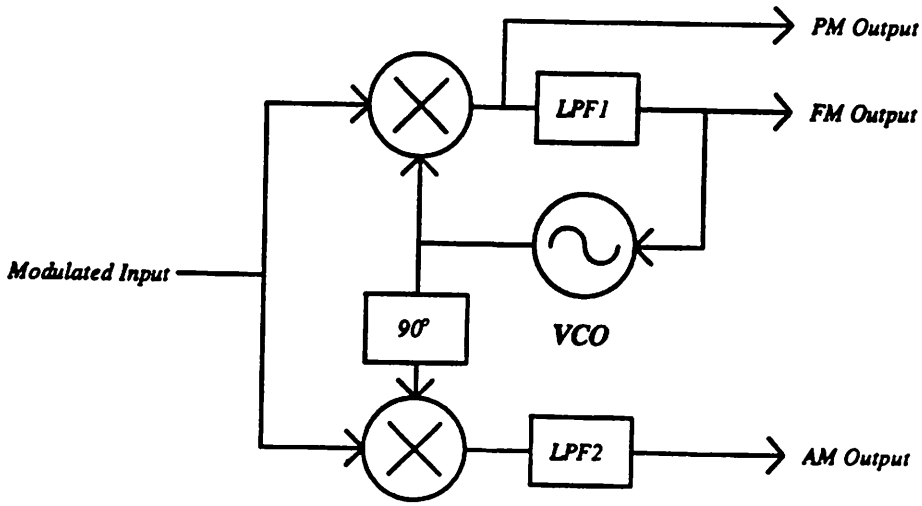

Figure 1.3 Demodulation outputs from a PLL.

Oscillator circuits can be classified into two groups: *relaxation* oscillators and *harmonic* (or *sinusoidal*) oscillators. While relaxation oscillators do not require resonating devices such as crystals, dielectric resonators, or LC tanks to operate, they tend to have poorer phase noise characteristics for a given amount of power consumption. Harmonic VCOs with integrated resonating devices that do not require post production tuning allow for lower external parts count, smaller board space, and shorter production time, and therefore, provide an attractive lower-cost solution to high volume applications compared to discrete designs.

Higher levels of integration on the transceiver blocks, for example, integrating a VCO with a downconverter, afford lower overall system power consumption by reducing the number of impedance-matched signal lines.

As the frequency of interest moves into the giga-hertz regime, device parasitics begin to introduce excess phase shift and affect proper oscillation build-up. The start-up criteria of the oscillators must be examined to ensure reliable oscillations.

2 Voltage-Controlled Oscillator Start-up

2.1 Oscillation Build-Up

The basic requirement for an oscillation build up is the existence of a pair of complex conjugate poles

$$p_{1,2} = \alpha \pm j\beta \qquad 2.1$$

in the right half of the s-plane, i.e., with $\alpha > 0$. The circuit is then unstable about its operating point and can produce a growing sinusoidal signal

$$y(t) = y_0 e^{\alpha t} \cos(\beta t) \qquad 2.2$$

when subjected to an excitation (due to power supply turn-on transients or noise in the circuit) where y_0 is determined by initial conditions. The amplitude of the signal will continue to grow until it begins to limit due to the non-linearities of the circuit.

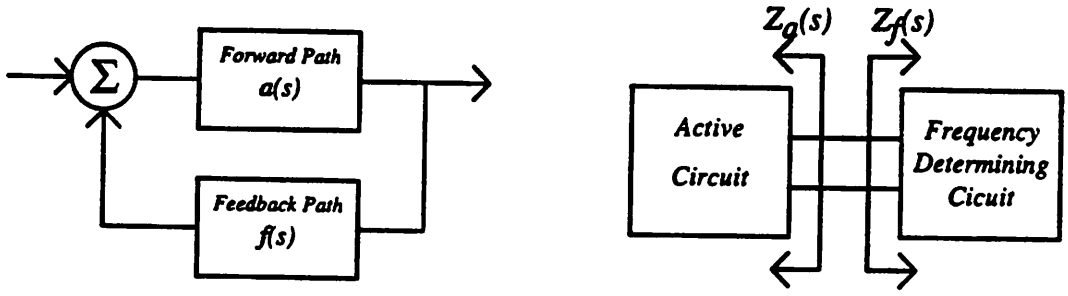

(a) Feedback Model (b) Negative-Resistance Model

Fig. 2.1 Harmonic Oscillator Models

Oscillation build-up can be predicted by studying linear behavior of the oscillators (a study of their pole locations) using either the feedback model or the negative resistance model (Fig. 2.1). One model is preferred over the other depending on the oscillator configuration. We shall briefly discuss the feedback model and then concentrate on the negative resistance model because of its simplicity and its natural extension to a steady state oscillator behavior analysis as shown by Kurokawa [Kurokawa69].

In the feedback model in Fig. 2.1a, the oscillator circuit is separated into the forward and feedback paths. The poles of the circuit can be determined by the roots of the characteristic equation

$$1 - T(s) = 0 \qquad 2.3$$

where $T(s)$ the loop gain is the product of the transfer functions of the forward and feedback paths $a(s).f(s)$. The fulfillment of the following criteria has often been used to as an indication that the circuit is unstable.

$$|T(\omega_z)| > 1 \qquad \angle T(\omega_z) = 0 \pm 2\pi n \quad (n = 0,1,2,...) \qquad 2.4$$

ω_z denotes the frequency at which the total phase-shift through the forward and feedback paths is zero. Although this condition is necessary, it is, however, not sufficient to ensure an oscillation build-up especially in the case where (2.4) is satisfied at multiple frequencies [Nguyen].

In the negative-resistance model in Fig. 2.1b, the oscillator circuit is separated into a one-port active circuit and a one-port frequency determining circuit, assuming that the steady-state current entering the active circuit is near-sinusoidal, that are characterized by their impedances $Z_a(s)$ and $Z_f(s)$, respectively. The characteristic equation of the oscillator is given by the expression

$$Z_a(s) + Z_f(s) = 0. \qquad 2.5$$

The frequency determining circuit is usually a linear time-invariant resonant circuit while the active circuit is nonlinear to provide amplitude limiting.

The following condition has been used to indicate circuit instability [Maas]:

$$R_a(\omega_x) + R_f(\omega_x) < 0 \qquad 2.6a$$

$$X_a(\omega_x) + X_f(\omega_x) = 0 \qquad 2.6b$$

where $R_a = \mathrm{Re}\{Z_a\}$, $R_f = \mathrm{Re}\{Z_f\}$, $X_a = \mathrm{Im}\{Z_a\}$, and $X_f = \mathrm{Im}\{Z_f\}$ are the respective resistances and reactances of Z_a and Z_f and ω_x denotes the frequency at which the total reactive component equals zero. However, it has been shown that (2.6) is not a sufficient

condition for oscillation build-up particularly in the case where (2.6) is satisfied at multiple frequencies [Nguyen].

It will be shown below heuristically that there is another necessary condition in addition to 2.6a and 2.6b for a well-behaved oscillation. Assuming again that the steady-state current going into the active circuit is near-sinusoidal, the topology that is known to result in a well-behaved oscillator is a series *RLC* resonator driven by a current-controlled negative resistance (ICNR) (see section 2.3). With the simplifying assumptions that the reactive component of the active circuit, $X_a(\omega)$, can be lumped into $X_f(\omega)$ (resulting in an equivalent inductance, L_{eq}, and an equivalent capacitance, C_{eq}), and that the resistive component of the active circuit is largely frequency independent, i.e. $\frac{\partial R_a(\omega)}{\partial \omega} << 1$, then

$$Z_a(s) = R_a \text{ and } Z_f(s) = R_f + s \cdot L_{eq} + \frac{1}{s \cdot C_{eq}}.$$

We have $X_T(\omega) = X_a(\omega) + X_f(\omega) = \omega \cdot L_{eq} - \frac{1}{\omega \cdot C_{eq}}$.

However,

$$\frac{\partial X_T(\omega)}{\partial \omega} = L_{eq} + \frac{1}{\omega^2 \cdot C_{eq}} > 0$$

which is always positive. Hence, in addition to 2.6a and 2.6b, for the existence of a series resonance in the region of ω_x, it is necessary that

$$\frac{\partial (X_a(\omega_x) + X_f(\omega_x))}{\partial \omega} > 0. \qquad 2.6c$$

Alternatively, if the voltage across the active circuit is near-sinusoidal, the active and frequency determining circuits should be characterized by their respective admittances $Y_a(s)$ and $Y_f(s)$. The topology that is known to result in a well-behaved oscillator is a parallel *RLC* resonator driven by a voltage-controlled negative resistance (VCNR) (see section 2.3). The corresponding characteristic equation of the oscillator is then given by the expression

$$Y_a(s) + Y_f(s) = 0 \qquad 2.7$$

and the dual of condition (2.6), for the existence of a parallel resonance in the region of ω_x, is

$$G_a(\omega_x) + G_f(\omega_x) < 0 \qquad 2.8a$$

$$B_a(\omega_x) + B_f(\omega_x) = 0 \qquad 2.8b$$

$$\frac{\partial\,(B_a(\omega_x) + B_f(\omega_x))}{\partial\,\omega} > 0 \qquad 2.8c$$

where $G_a = \mathrm{Re}\{Y_a\}$, $G_f = \mathrm{Re}\{Y_f\}$, $B_a = \mathrm{Im}\{Y_a\}$, and $B_f = \mathrm{Im}\{Y_f\}$ are the respective conductances and susceptances of $Y_a(s)$ and $Y_f(s)$.

2.1.1 Guidelines for Proper Oscillation Start-Up

As a general guideline, conditions 2.4, 2.6 or 2.8 are valid for predicting proper oscillation start-ups if they are satisfied at one frequency only. Proper oscillator start-up behavior may be further confirmed with the Nyquist and root-locus analyses of 2.3, 2.5, or 2.7 [Nguyen]. Root-locus analysis is particularly useful for additional insight of the oscillator circuit operation such as the presence of multi-oscillations.

2.2 Oscillator Steady-State Behavior

While linear analyses are useful for analyzing oscillation start-up, they are no longer valid as the oscillation continues to grow and the non-linearities of the circuit become important. Nonlinear analysis can be used to predict the oscillation amplitude and the spectral purity of the output signal. Nonlinear analysis of oscillator behavior can be somewhat simplified by assuming a near sinusoidal oscillation [Clarke-Hess, Kurokawa]. Kurokawa showed that for a steady-state oscillation with a near sinusoidal current the following condition holds

$$R_a(\omega_o, A_o) + R_f(\omega_o) = 0 \qquad 2.9a$$

$$X_a(\omega_o, A_o) + X_f(\omega_o) = 0 \qquad 2.9b$$

where ω_o is the steady state oscillation frequency and A_o is the steady state oscillation amplitude. The impedance of the active circuit, $Z_a = R_a + jX_a$, is generally a function of the oscillation frequency and the oscillation amplitude because of its nonlinear nature. It needs to be emphasized that in (2.9) R_a and X_a, the resistance and reactance of the active circuit are evaluated at the fundamental frequency, ω_o. ω_z, the frequency at which the total phase-shift through the forward and feedback paths is zero, and ω_x, the frequency at which the total reactive or susceptive component equals zero, are in general not equal to ω_o. However, for resonant circuits with high Qs, ω_z and ω_x are good approximations to the steady state oscillation frequency.

If instead the steady state voltage is near sinusoidal, then the dual of (2.9) below holds

$$G_a(\omega_o, A_o) + G_f(\omega_o) = 0 \qquad 2.10a$$

$$B_a(\omega_o, A_o) + B_f(\omega_o) = 0 \qquad 2.10b$$

Again, it needs to be emphasized that in (2.10) G_a and B_a, the conductance and susceptance of the active circuit are evaluated at the fundamental frequency, ω_o.

2.3 Voltage-Controlled Oscillator Resonator Topologies

In order to realize reliable oscillators, it is important to choose the appropriate frequency-determining circuit (resonator) that interacts with a given active circuit. We shall concentrate on one-port active circuits such as tunnel diodes or other circuits whose I-V characteristics contain a negative resistance region since they lend themselves to the negative resistance model.

One-port active circuits generally fall under two categories namely voltage-controlled negative resistances (VCNR) and current-controlled negative resistances (ICNR). An active circuit is a VCNR if the port current is a single valued function of the port voltage. An emitter-coupled pair with positive feedback (figure 2.2a) is an example. The normalized I-V characteristic of the circuit, with $\frac{i}{I_{EE}} = \frac{1}{1+e^{b}}$, where $b = \frac{v}{V_T}$, is shown in figure 2.2b.

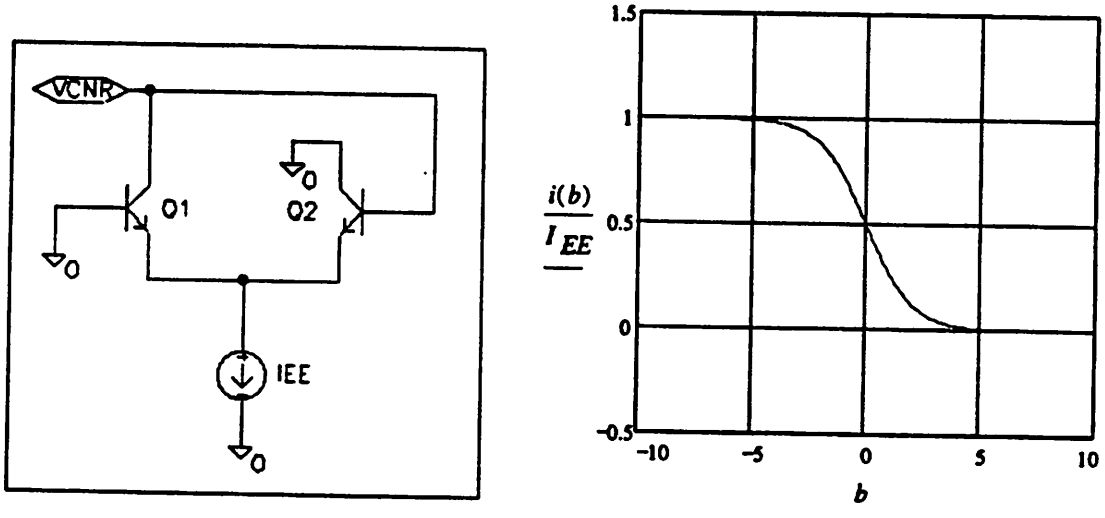

Figures 2.2a ECP with positive feedback (left) & 2.2b I-V characteristic of ECP (right).

It has been shown that the most appropriate frequency-determining circuit for a VCNR that results in a well-behaved sinusoidal oscillator is a parallel *RLC* resonant circuit, and that for an ICNR is a series *RLC* resonant circuit [Nguyen]. Figure 2.3a

shows commonly used arrangement of a VCNR with a varactor-tuned parallel *RLC* resonant circuit where $g_l < 0$ models the active circuit that overcomes the losses in the resonant circuit. The varactor, c_v, whose capacitance is a function of its reverse bias voltage is used to tune the resonant frequency of the tank. c_c is a capacitor that ac-couples the varactor to the parallel tank.

Figure 2.3b shows the dual of figure 2.3a, an ICNR, with $h_l < 0$, driving a varactor-tuned series *RLC* resonant circuit.

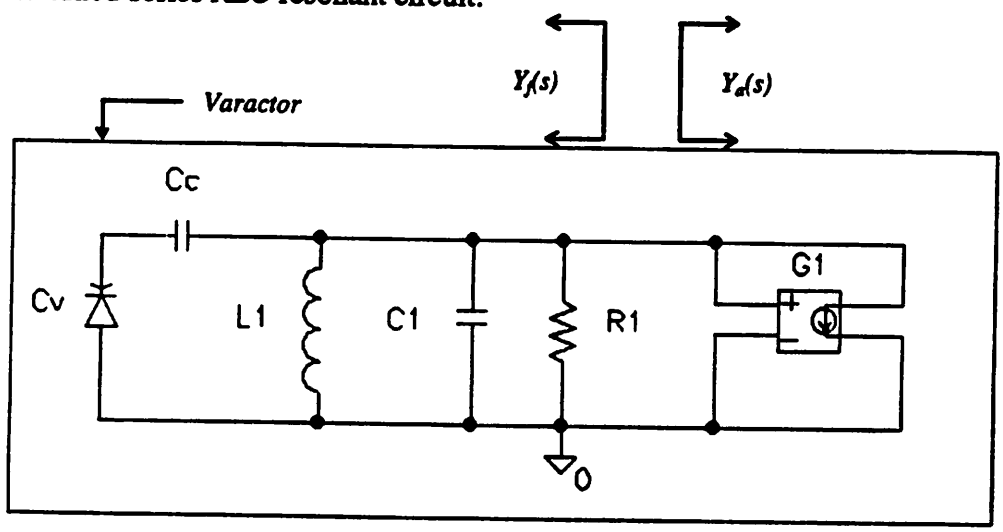

Figure 2.3a VCNR with varactor-tuned parallel resonant tank.

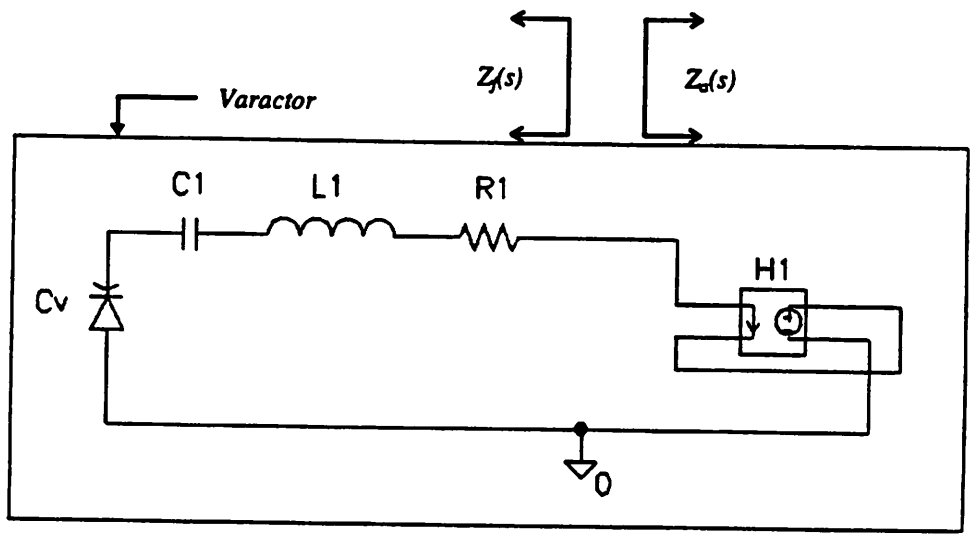

Figure 2.3b ICNR with varactor-tuned series resonant tank.

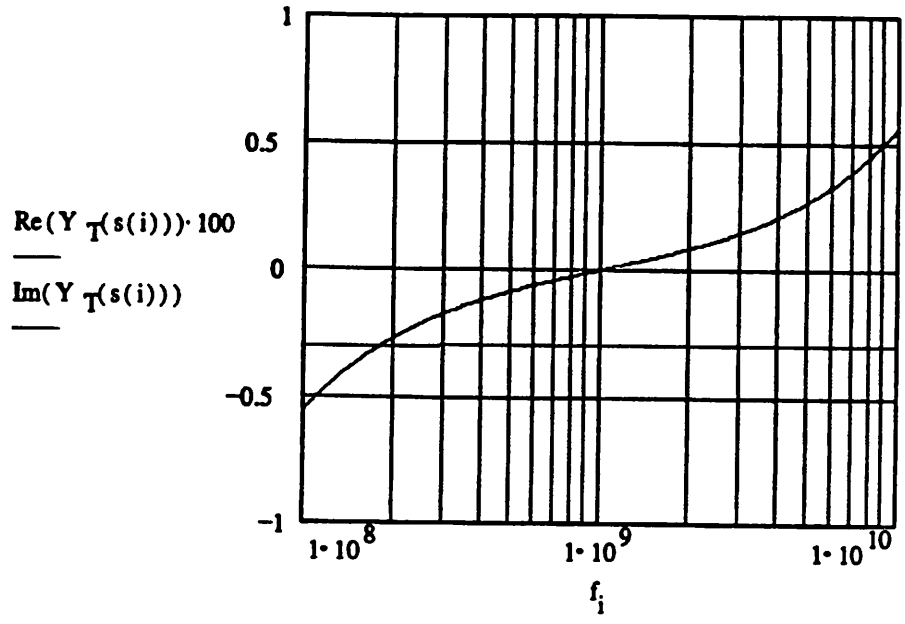

Figure 2.4 Admittance plot of circuit in figure 2.3a.

The admittance of the circuit in figure 2.3a, $Y_T(s) = Y_a(s) + Y_f(s)$, where

$$Y_a(s) = g_1,$$

$$\text{with } g_1 = -\frac{4}{r_1}, \text{ and}$$

$$Y_f(s) = s \cdot (c_1 + c_v) + \frac{1}{s \cdot l_1} + \frac{1}{r_1}, \text{ assuming } c_c >> c_v, \qquad 2.11$$

is plotted in figure 2.4 with c_1 = 4pF, c_v= 5pF, l_1= 2.8nH and, r_1= 1Kohm. The values of c_1, c_v, and l_1 are chosen for a resonant frequency of 1GHz. g_1 is set equal to $-\frac{4}{r_1}$ so that the initial loop gain is 4 which results in reliable oscillations [Meyer]. The susceptance of the active circuit is not modeled under the assumption that, for small-signal analysis, it can be lumped into the frequency-determining circuit. It would appear that the we have a well-behaved circuit since condition 2.8 is satisfied only at one frequency.

2.3.1 Off-Chip Resonators

The circuit in figure 2.3a adequately models an oscillator for low frequency operation. However, at higher operating frequencies where parasitics are on the same order as the resonant tank components, this may no longer be true since parasitics may significantly affect the operation of an oscillator. In the case where the active circuit is contained in a package and is connected to the resonant circuit externally, the impact of package parasitics become more pronounced. This is also the case for packaged varactors where the lead and bond-wire inductances increase the equivalent capacitance. What is of more significance is the presence of undesired oscillation modes due to these parasitics.

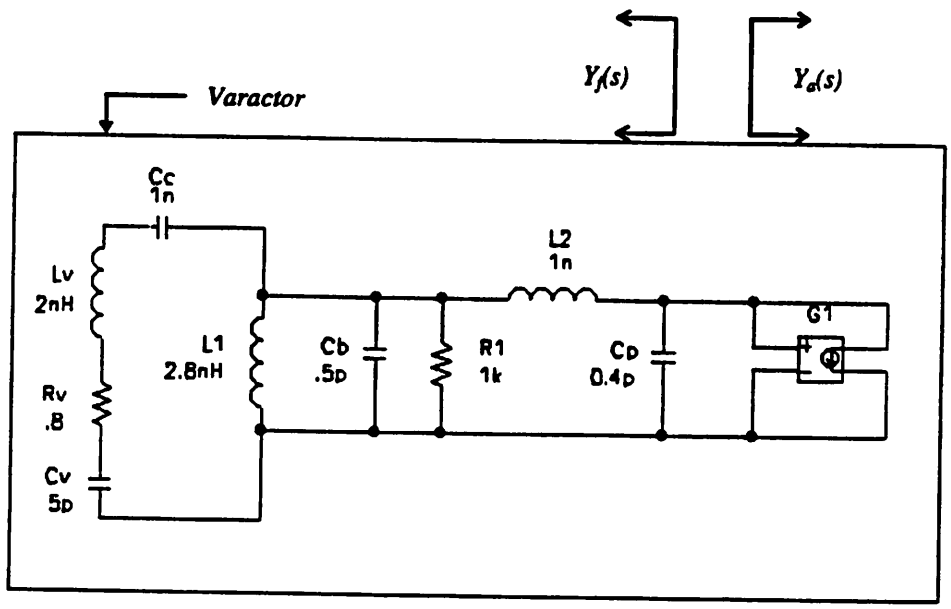

Figure 2.5 Equivalent circuit of figure 2.3a with package parasitics.

The equivalent circuit of figure 2.3a including package parasitics of the varactor and the active circuit is shown in figure 2.5. l_v models the package lead and bond-wire inductances of the varactor while r_v models the resistive losses. c_b models the parasitic capacitances of the board, varactor, and l_1 while c_p and l_2 model the parasitics associated with the package that contains the active circuit.

The sum of admittances, $Y_T(s) = Y_a(s) + Y_f(s)$, where

$$Y_a(s) = g_1,$$

with, $g_1 = -4 \cdot G_f(j\omega_0)$, and,

$$Y_f(s) = s \cdot c_p + \cfrac{1}{s \cdot l_2 + \cfrac{1}{s \cdot c_b + \cfrac{1}{s \cdot l_1} + \cfrac{1}{s \cdot l_v + r_v + \cfrac{1}{s \cdot c_v}} + \cfrac{1}{r_1}}}, \text{ assuming } c_c >> c_v, \qquad 2.12$$

is plotted in figure 2.6.

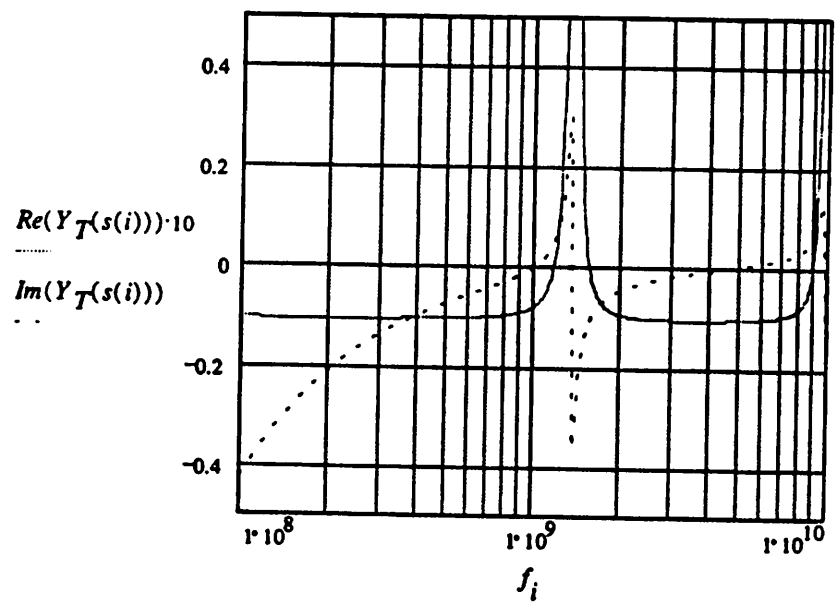

Figure 2.6 Admittance of circuit in figure 2.5

It can be seen from the admittance plot (figure 2.6) of the circuit in figure 2.5 that there are multiple resonances present. There are two parallel resonances; one at 1 GHz (desired) and another at 4.3 GHz (undesired). Condition 2.8 is satisfied at these two frequencies. The resonance at 4.3 GHz is due to the mode associated with $\frac{1}{s \cdot c_p} // (s \cdot l_2 + (\frac{1}{s \cdot c_b} // s \cdot l_1 // (s \cdot l_v + \frac{1}{s \cdot c_v})))$ which would not exist in the absence of l_2 and l_v. There are also series resonances occurring at 1.3 GHz and at around 10 GHz. The output waveform is shown in figure 2.7a. From the expanded view of the

Figure 2.7a Output waveform of circuit in figure 2.5.

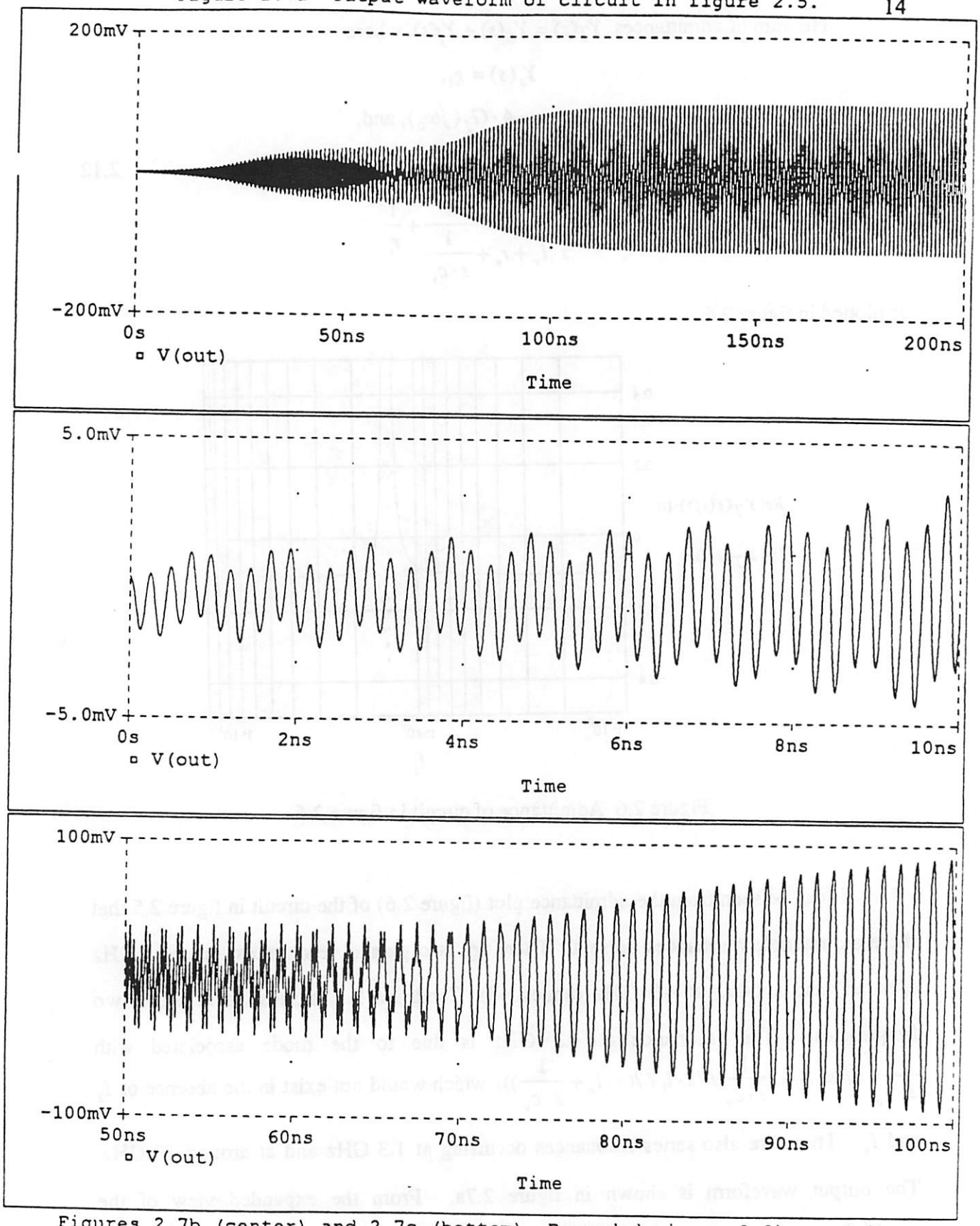

Figures 2.7b (center) and 2.7c (bottom) Expanded views of figure 2.7a.

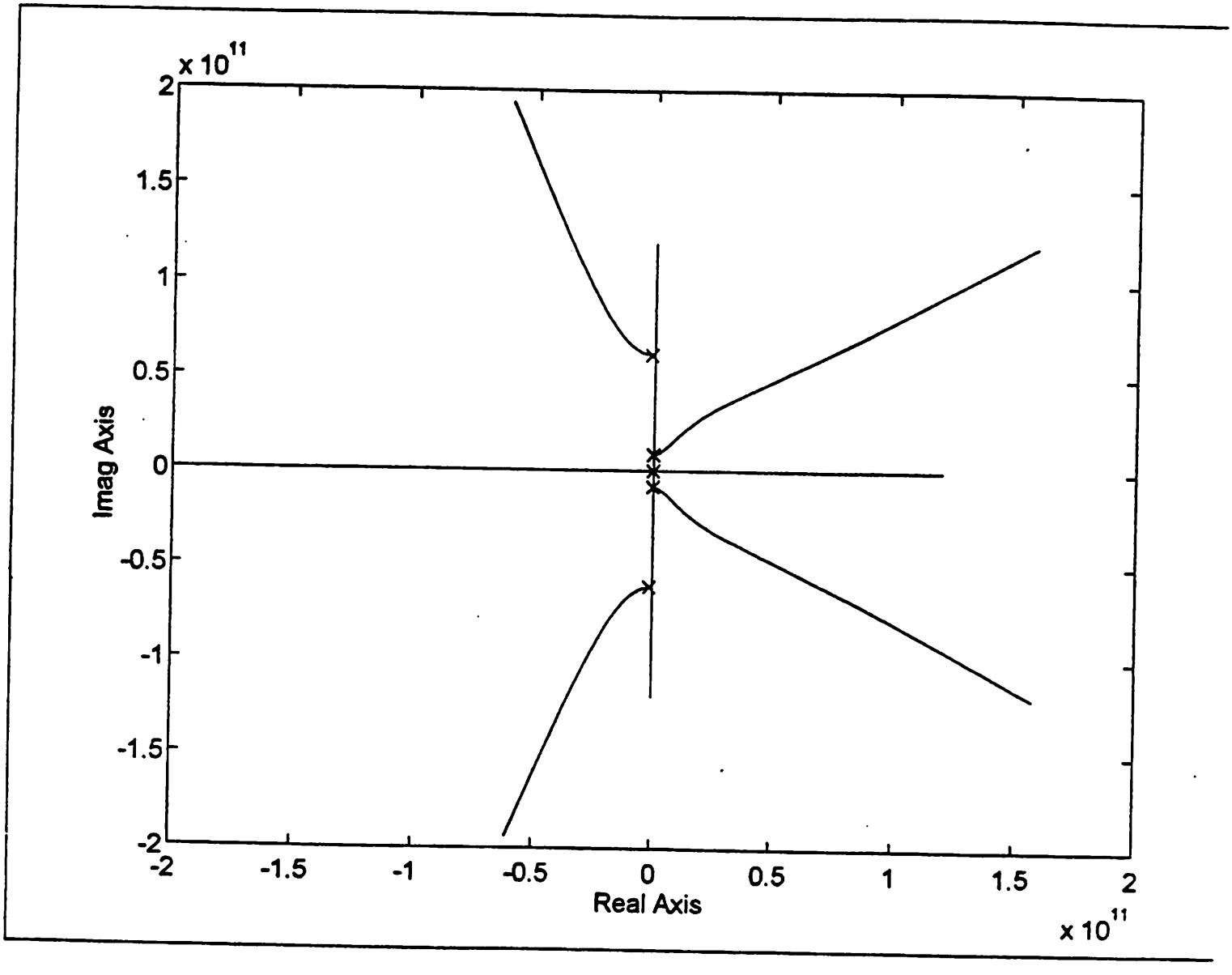

Figure 2.8 Loci of poles of circuit of figure 2.5.

build-up of figure 2.7a (figure 2.7b), we can see that the circuit initially oscillates at two different frequencies---at 1 GHz and at 4.3 GHz. The oscillations continue to build-up until a certain point when the 1 GHz mode dominates (figure 2.7c).

The poles of the circuit are given by the roots of equation 2.13. The loci (not including the effects of the zeroes of the circuit) of the poles as a function of g_1 are plotted in figure 2.8. There is one (lower frequency) pair of complex conjugate poles located on the $j\omega$ axis and an other (higher frequency) pair located close to the $j\omega$ axis. We expect the higher frequency mode to eventually die out. However, the possibility for steady-state multi-oscillations is high if this higher frequency mode is less damped. This agrees with the output waveform of the circuit.

$$a_5 \cdot s^5 + a_4 \cdot s^4 + a_3 \cdot s^3 + a_2 \cdot s^2 + a_1 \cdot s + a_0 = 0, \text{ where}$$

$$a_5 = r_1 \cdot l_1 \cdot l_2 \cdot l_v \cdot c_v \cdot c_b$$

$$a_4 = l_1 \cdot l_2 \cdot c_v \cdot (c_b \cdot r_1 \cdot r_v + l_v)$$

$$a_3 = r_1 \cdot l_1 [l_2 \cdot (c_b + c_v) + l_v \cdot c_v] + l_2 \cdot c_v \cdot (r_1 \cdot l_v + r_v \cdot l_1)$$

$$a_2 = r_1 \cdot r_v \cdot c_v \cdot (l_1 + l_2) + l_1 \cdot l_2$$

$$a_1 = r_1 \cdot (l_1 + l_2)$$

$$a_0 = 0 \qquad 2.13$$

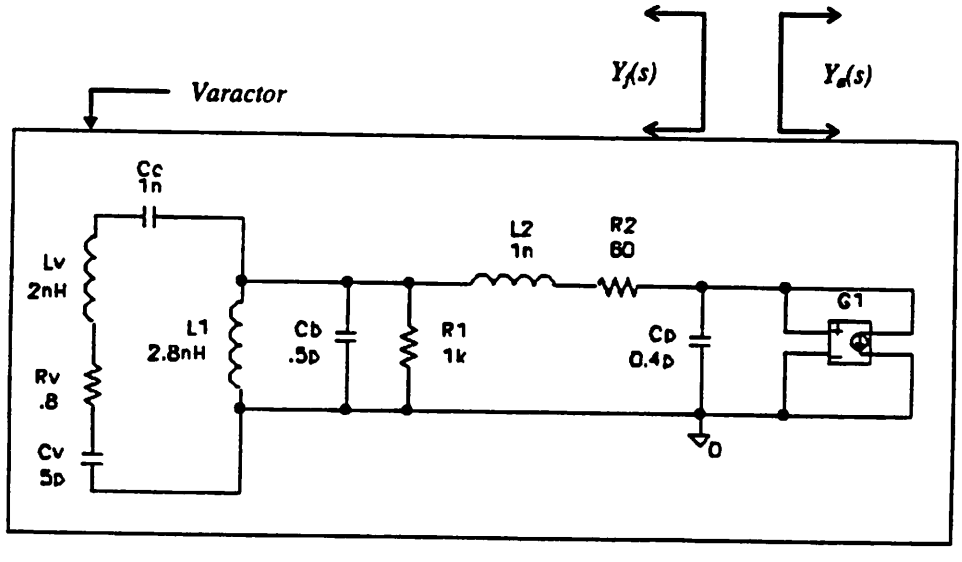

Figure 2.9 Circuit in figure 2.5 with damping resistor in series with package parasitic inductance.

It is apparent that the parasitic inductances of packages can cause spurious oscillation modes. It would seem that there may be some way of damping the undesired oscillation modes. The circuit in figure 2.5 is shown with damping resistor, r_2, placed in series with the package parasitic inductance, l_2, in figure 2.9.

The sum of admittances of the circuit in figure 2.9, $Y_T(s) = Y_a(s) + Y_f(s)$, where

$$Y_a(s) := G_a,$$

with, $g_1 = -4 \cdot G_f(j\omega_0)$, and,

$$Y_f(s) = s \cdot c_p + \frac{1}{s \cdot l_2 + r_2 + \frac{1}{s \cdot c_b + \frac{1}{s \cdot l_1} + \frac{1}{s \cdot l_v + r_v + \frac{1}{s \cdot c_v}} + \frac{1}{r_1}}}, \text{ assuming } c_c >> c_v, \qquad 2.14$$

is plotted in figure 2.10. The value of r_2, 60 Ohm, is chosen such that condition 2.8 is now satisfied only at the desired oscillation frequency, 1 GHz; hence, eliminating the mode associated with $\frac{1}{s \cdot c_p} // (s \cdot l_2 + (\frac{1}{s \cdot c_b} // s \cdot l_1 // (s \cdot l_v + \frac{1}{s \cdot c_v})))$.

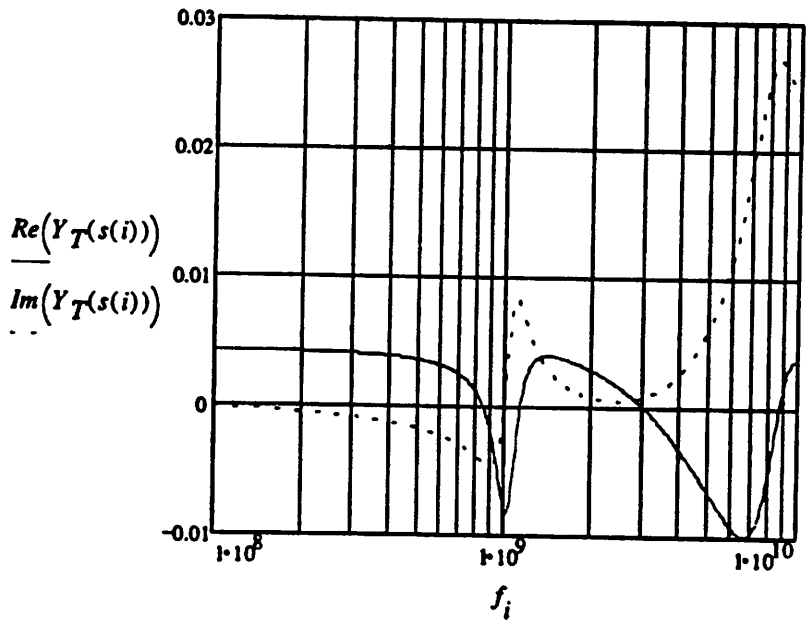

Figure 2.10 Admittance of circuit in figure 2.9.

The poles of the circuit in figure 2.9 are given by the roots of

$$a_5 s^5 + a_4 s^4 + a_3 s^3 + a_2 s^2 + a_1 s + a_0 = 0 \text{, where}$$

$$a_5 = r_1 \cdot l_1 \cdot l_2 \cdot l_v \cdot c_v \cdot c_b$$

$$a_4 = l_1 \cdot c_v \cdot \left[r_1 \cdot r_2 \cdot c_b \cdot l_v + l_2 \cdot \left(c_b \cdot r_1 \cdot r_v + l_v \right) \right]$$

$$a_3 = r_1 \cdot l_1 \left[l_2 \cdot \left(c_b + c_v \right) + l_v \cdot c_v + r_2 \cdot r_v \cdot c_v \cdot c_b \right] + l_2 \cdot c_v \cdot \left(r_1 \cdot l_v + r_v \cdot l_1 \right) + r_2 \cdot l_1 \cdot l_v \cdot c_v$$

$$a_2 = r_1 \cdot r_v \cdot c_v \cdot \left(l_1 + l_2 \right) + l_1 \cdot l_2 + r_2 \cdot \left[l_1 \left[c_v \cdot \left(r_v + r_1 \right) + c_b \cdot r_1 \right] + r_1 \cdot c_v \cdot l_v \right]$$

$$a_1 = r_1 \cdot \left(l_1 + l_2 \right) + r_2 \cdot \left(r_1 \cdot r_v \cdot c_v + l_1 \right)$$

$$a_0 = r_1 \cdot r_2 \qquad 2.15$$

The loci (not including the effects of the zeroes of the circuit) of the poles as a function of g_l are plotted in figure 2.11. It can be seen that the complex conjugate pair of poles associated with the undesired oscillation mode due to the parasitic package inductance are pushed further into the left-half plane i.e. that mode is damped. The output waveform of the circuit in figure 2.9, shown in figure 2.12a, is a well-behaved build-up. An expanded view of the steady-state waveform is shown in figure 2.12b.

In figure 2.13, the phase of the frequency-determining part, $Y_f(j\omega)$, around the desired oscillation frequency, 1 GHz, with and without the addition of the damping resistor, r_2, is compared. We find that the phase of the frequency-determining part has been significantly affected by the addition of the damping resistor, r_2. In particular, the slope of the phase of $Y_f(j\omega)$ has been lowered. This corresponds to a degradation in the phase-noise performance of the oscillator since the slope of the phase of $Y_f(j\omega)$ is proportional to the tank Q (chapter 3).

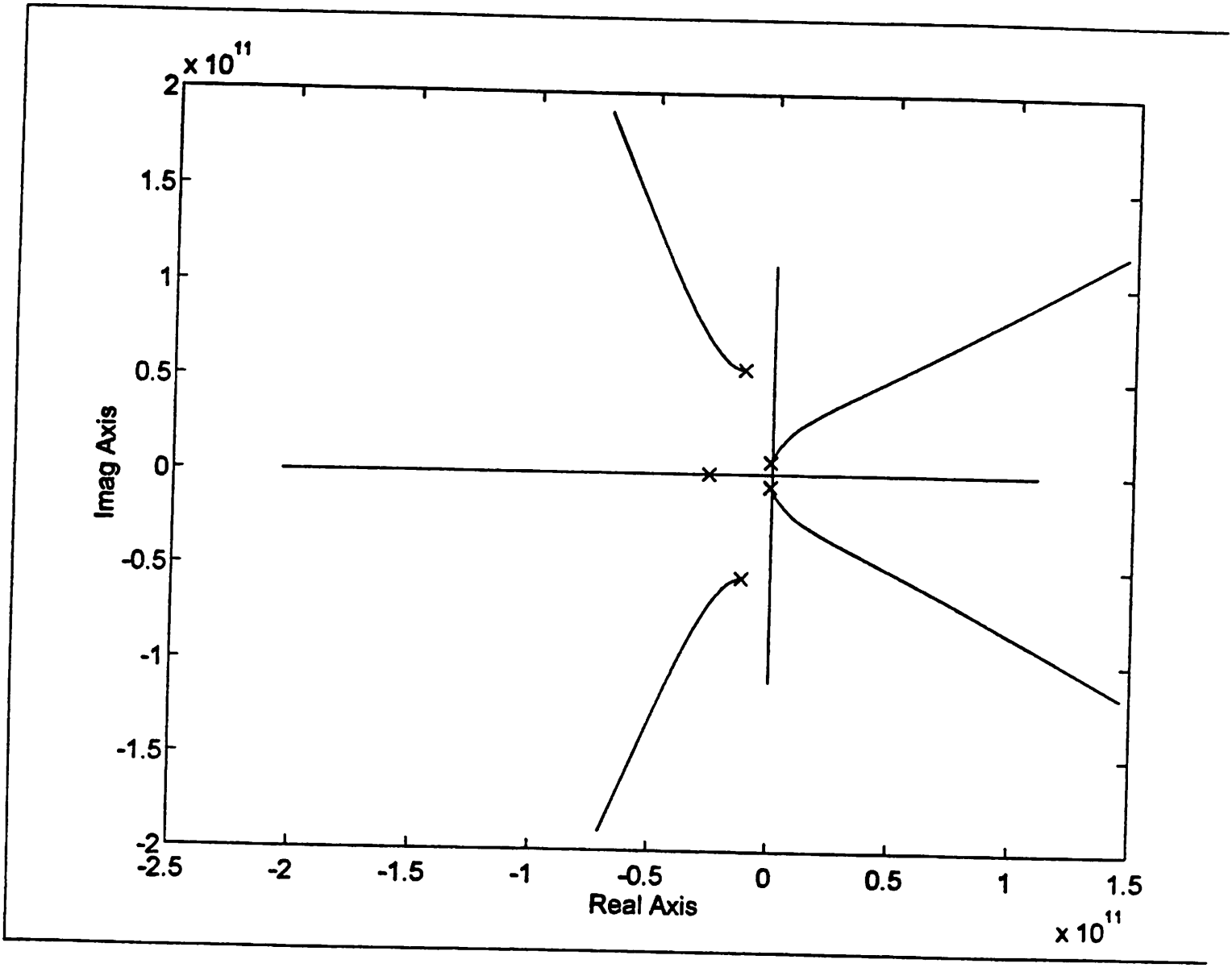

Figure 2.11 Loci of poles of circuit of figure 2.9.

Figure 2.12a Output waveform of circuit in figure 2.9.

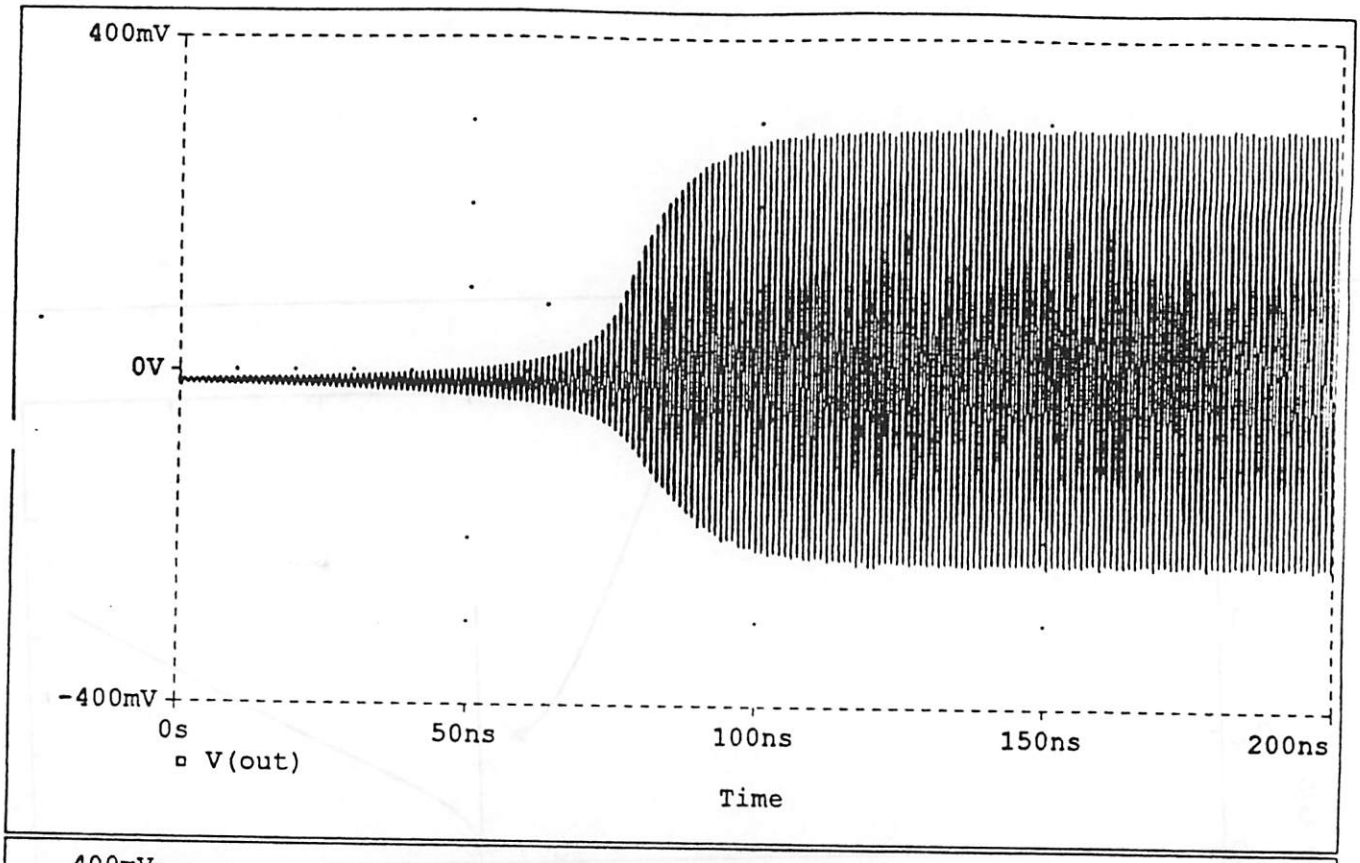

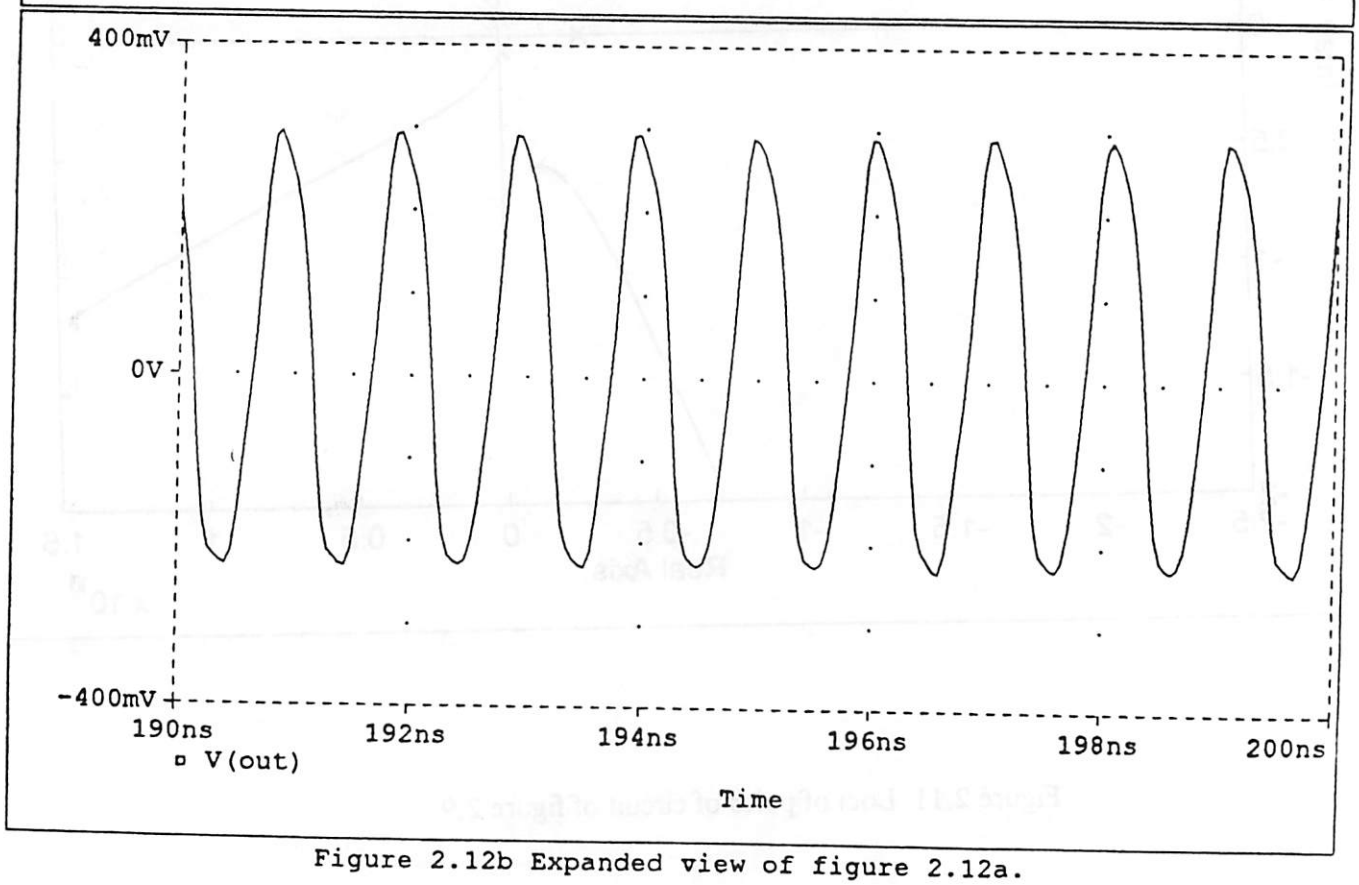

Figure 2.12b Expanded view of figure 2.12a.

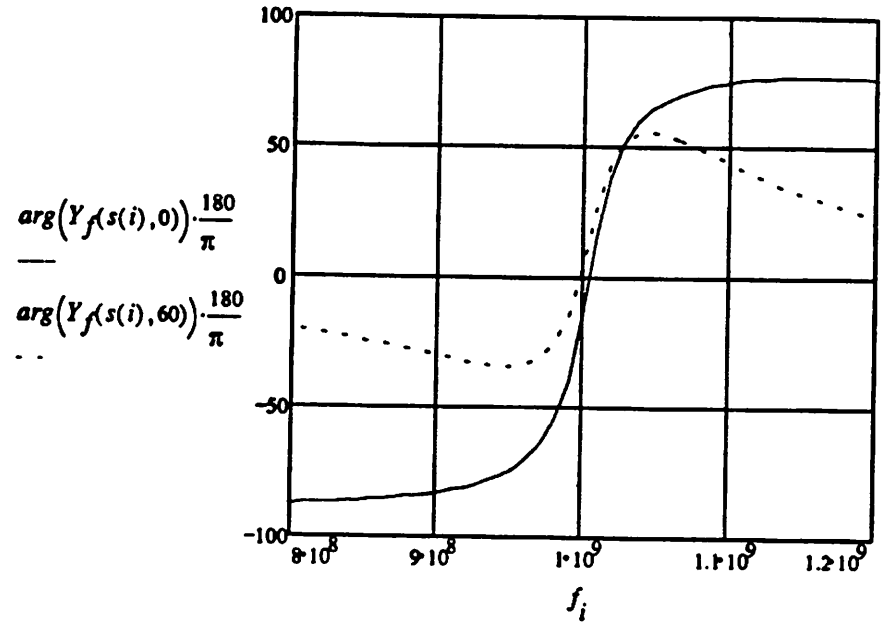

Figure 2.13 Phase of $Y_f(j\omega)$ in circuit of figure 2.9 with $r_2 = 0$ and $r_2 = 60$.

Resonator topologies which require a smaller value of r_2 to ensure that condition 2.8 is satisfied only at the desired oscillation frequency are needed in order to minimize the effect of r_2 on the slope of the phase of $Y_f(j\omega)$.

Figure 2.14 shows a parallel tank formed by c_b and l_1 which is tuned by the varactor capacitance, c_v. Please note that the parasitic inductance of the varactor, l_v, being in series with l_1, is now part of the tank inductance. This moves the second parallel resonance mode to 8.3 GHz as is shown in the admittance plot of the circuit in figure 2.15.

The value of r_2 required to ensure that condition 2.8 is satisfied only at the desired oscillation frequency, 1 GHz, is now 12. The slope of the phase of $Y_f(j\omega)$, as can be seen in figure 2.16, is lowered slightly from the undamped case. The phase noise performance of the circuit in figure 2.14 (compared to the circuit in figure 2.9) is, therefore, less affected by the damping effect of r_2. The tuning range of this circuit is, however, narrower than that of figure 2.9.

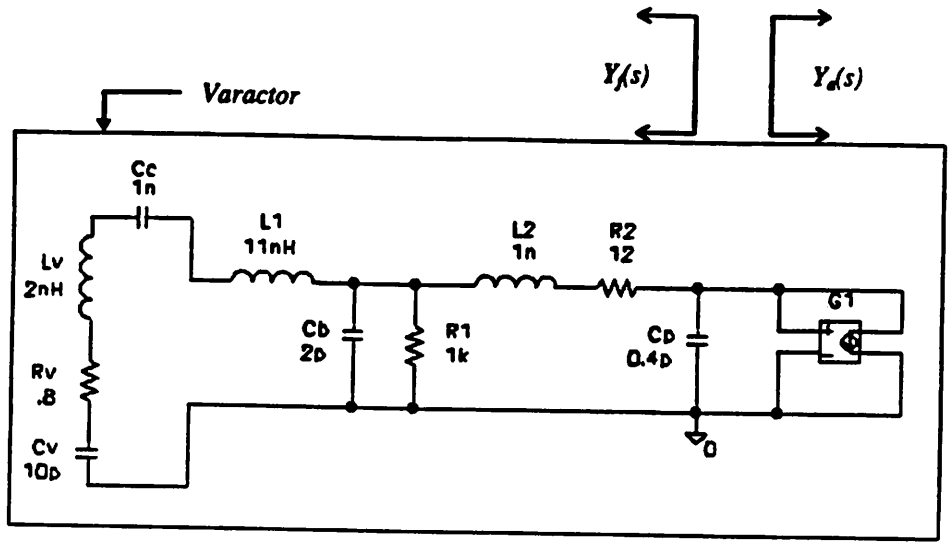

Figure 2.14 Parallel tank with varactor-tuned inductor.

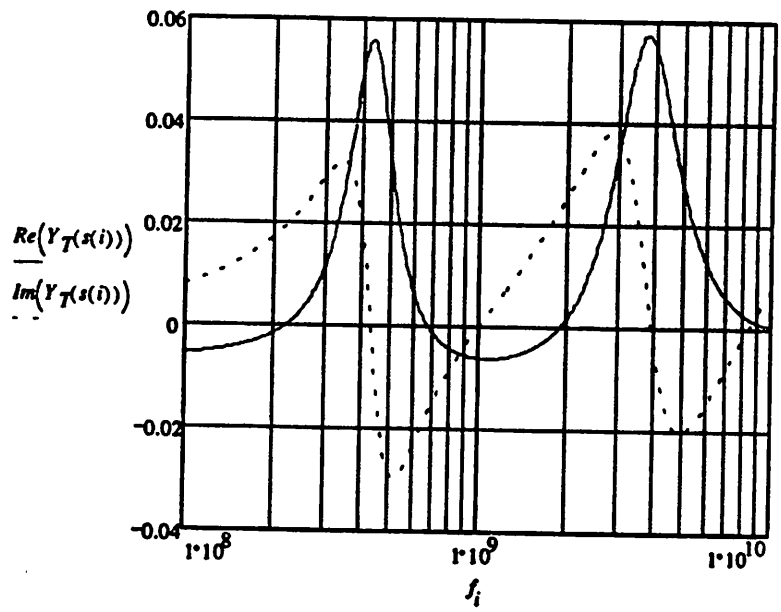

Figure 2.15 Admittance of circuit in figure 2.14.

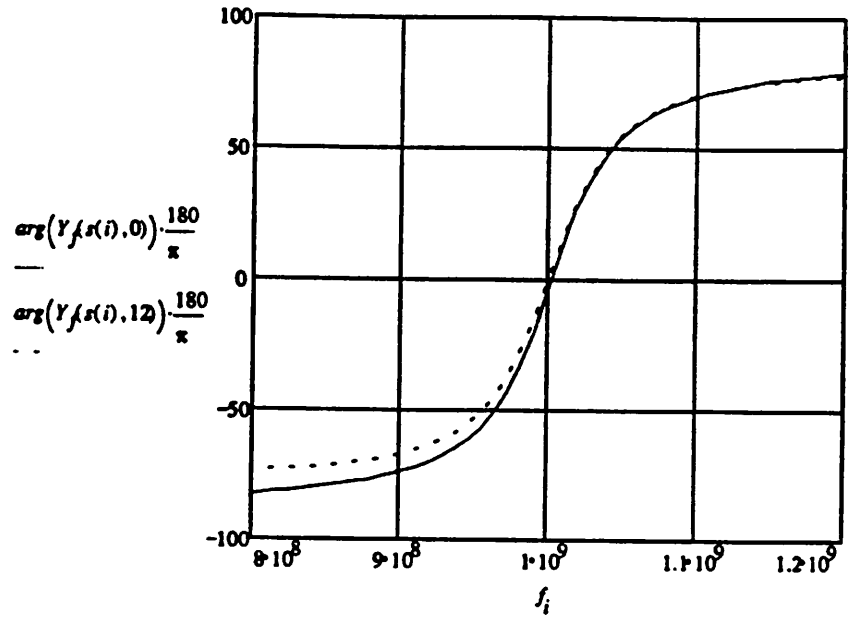

Figure 2.16 Phase of $Y_f(j\omega)$ in circuit of figure 2.14 with $r_2 = 0$ and $r_2 = 12$.

The poles of the circuit in figure 2.14 are given by the roots of

$$a_4 \cdot s^4 + a_3 \cdot s^3 + a_2 \cdot s^2 + a_1 \cdot s + a_0 = 0, \text{ where}$$

$$a_4 = r_1 \cdot l_2 \cdot l_v \cdot c_v \cdot c_b$$

$$a_3 = l_v \cdot c_v \cdot (r_1 \cdot r_2 \cdot c_b + l_2)$$

$$a_2 = l_v \cdot c_v \cdot (r_1 + r_2) + r_1 \cdot l_2 \cdot (c_b + c_v)$$

$$a_1 = l_2 + r_1 \cdot r_2 \cdot (c_b + c_v)$$

$$a_0 = r_1 + r_2 \qquad 2.16.$$

The order of the circuit in figure 2.14 is one less than that of figures 2.5 and 2.9. The loci (not including the effects of the zeroes of the circuit) of the poles as a function of g_l are plotted in figure 2.17. It can be seen that the complex conjugate pair of poles associated with the undesired oscillation mode due to the parasitic package inductance are pushed further into the left-half plane i.e. that mode is damped.

The output waveform of the circuit in figure 2.14, shown in figure 2.18a, is a well-behaved build-up. An expanded view of the steady-state waveform is shown in figure 2.18b.

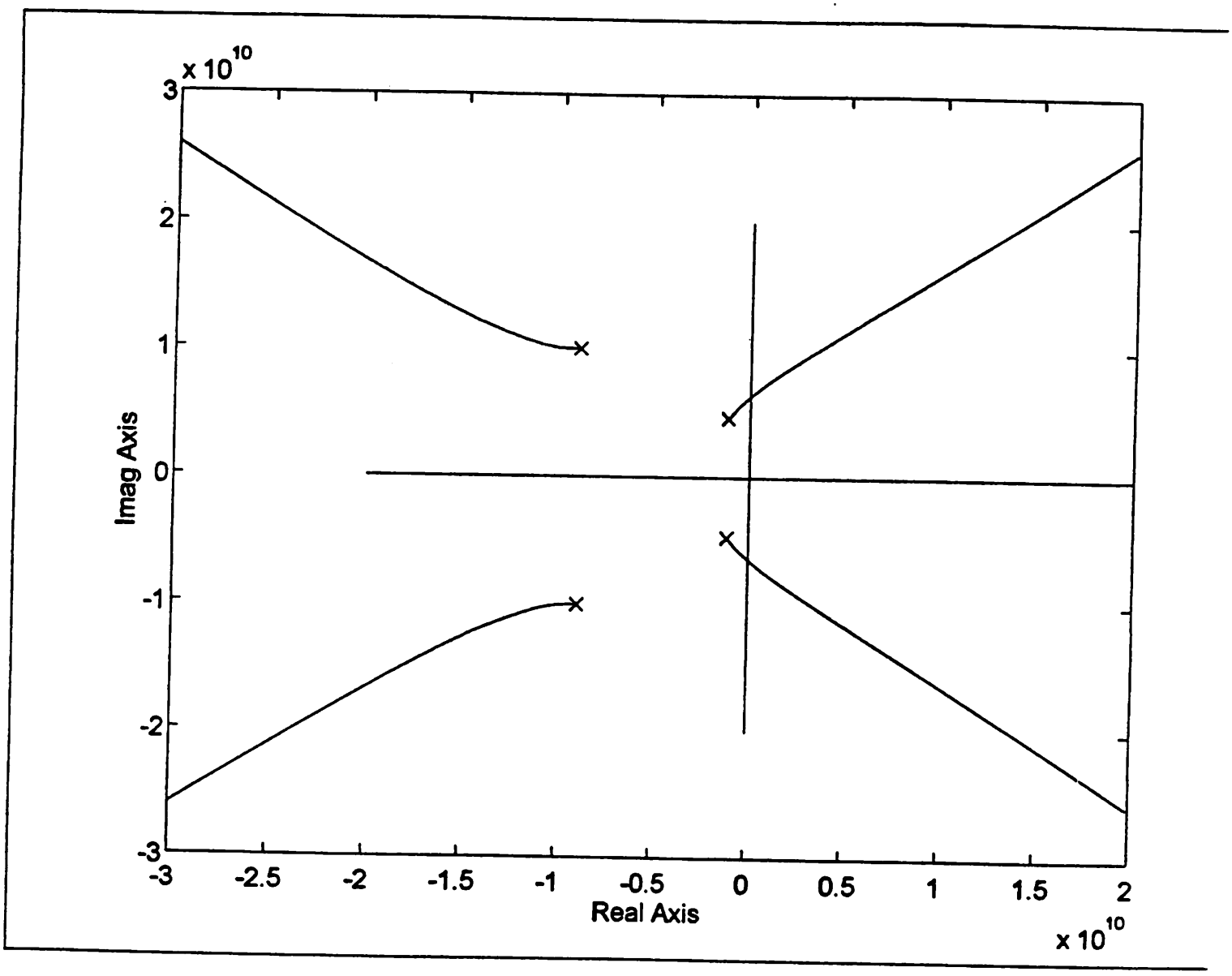

Figure 2.17 Loci of poles of circuit of figure 2.14.

Figure 2.18a Output waveform of circuit in figure 2.14.

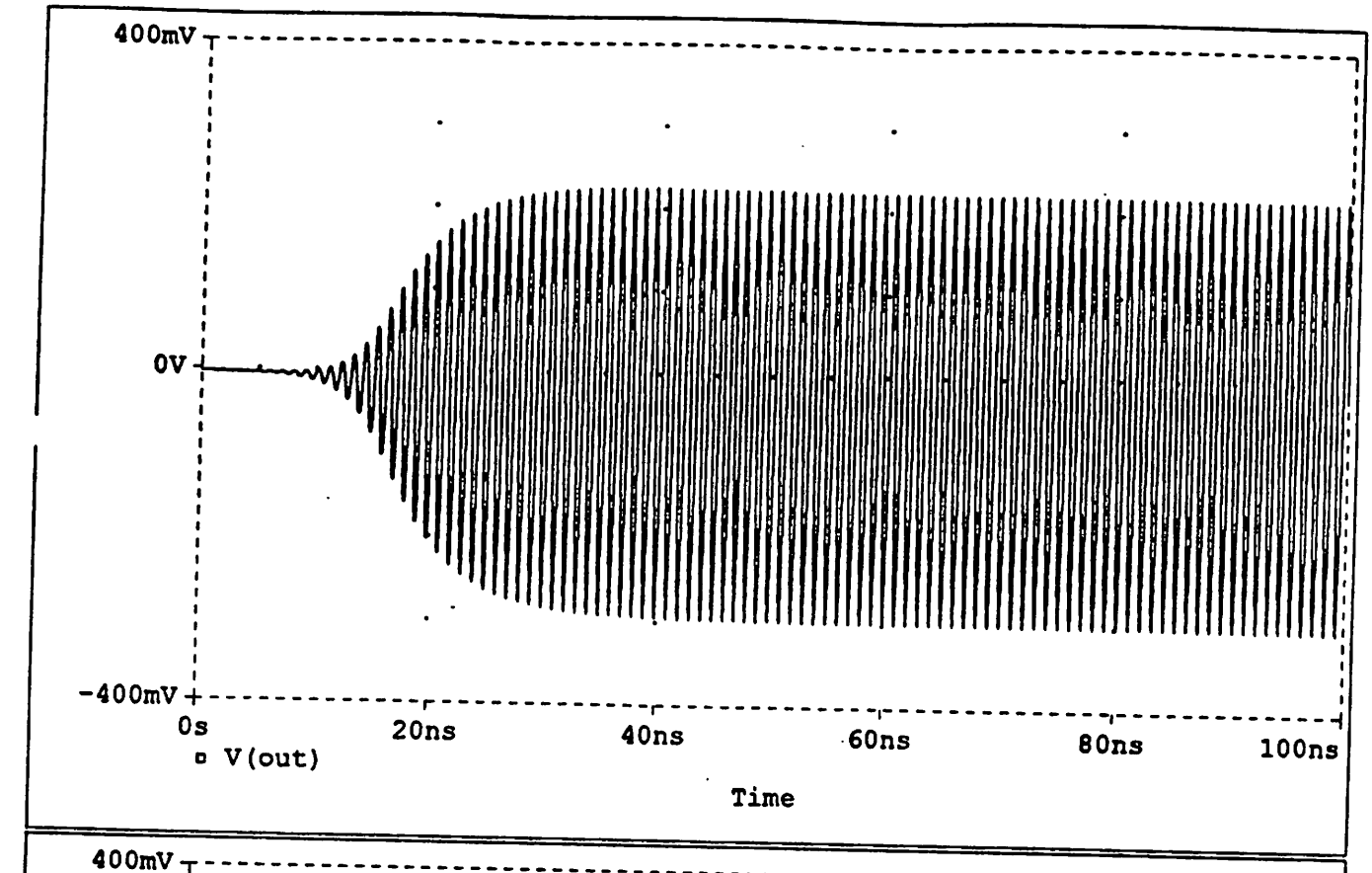

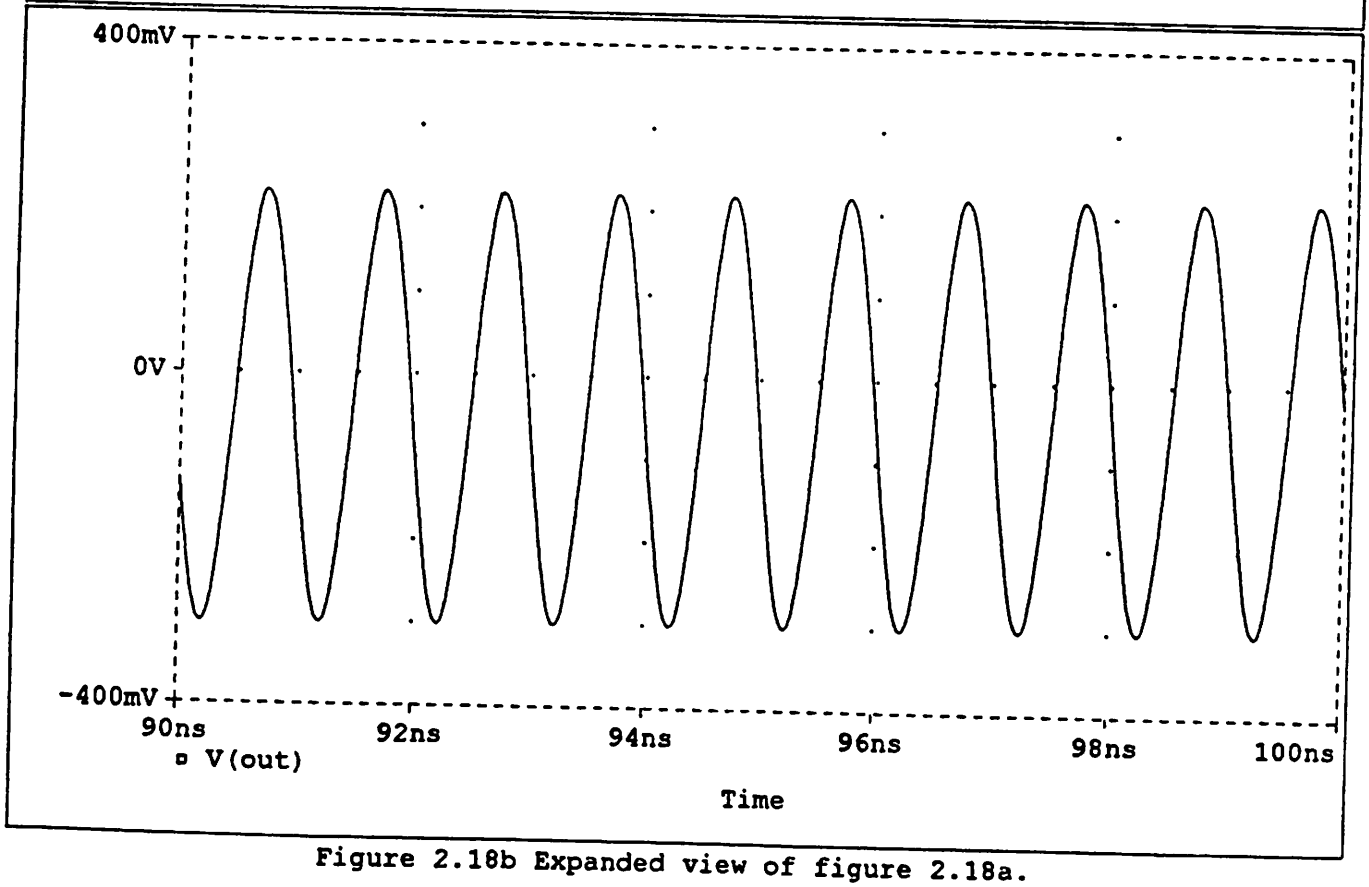

Figure 2.18b Expanded view of figure 2.18a.

2.3.2 Summary

It has been found that a resonator topology using external resonating elements which results in a well-behaved oscillator with undegraded phase noise performance needs to have the parasitic inductances as part of the tank. The most promising configuration in this regard is a series RLC resonant tank driven by an ICNR (figure 2.3b).

The alternative, an oscillator with on-chip resonator, has the appeal of having a controlled environment where the operation of the oscillator is largely unaffected by package parasitics. The phase noise performance of on-chip oscillators are, however, limited by the Q of the resonating elements available on-chip. In chapter 4, some measured results of a monolithic RF LC VCO shall be presented.

3 Low Phase-Noise Oscillators

3.1 Oscillator Noise

An oscillator can be naively viewed as a signal source as having an output at a single frequency, i.e. its spectrum is an infinitely narrow line (delta function) in the frequency domain. Real oscillators, even those of the highest quality, have imperfections which result in unwanted amplitude and phase modulation of the carrier.

In practice spurious phase modulation is more important than spurious amplitude modulation. Spurious amplitude modulation in oscillators is usually of a much lower level than spurious phase modulation, especially at offset frequencies close to the carrier. Moreover, spurious frequency or phase modulation of a local oscillator in a transceiver will be directly transferred to the signal that is subjected to the frequency conversion. Spurious amplitude modulation can be reduced by putting the carrier through limiting stages [Kurokawa68, Davenport].

In communication systems that uses coherent reception, it is desirable to have a reference oscillator with low noise since the coherent detection of these systems exhibit a degradation in error rate performance from ideal due to a phase discrepancy between the carrier of the received signal and the locally generated noisy reference [Matyas]. Low noise local oscillators are also important in receivers where a large interfering signal may reciprocally mix the local oscillator noise into the intermediate frequency (IF) band and, thus, desensitize the receiver. In the transmit chain, a noisy local oscillator may cause the transmitted output to have sufficient energy at some offset frequency from the carrier to interfere with other communication channels in its adjacent spectrum.

The oscillator noise spectral density, according to [Lindenmeier], in terms of known oscillator parameters, is

$$S(\Delta f) = \frac{1}{\pi \cdot \Delta f_{FM}} \cdot \left(\underbrace{\frac{1}{1+\left(\Delta f / \Delta f_{FM}\right)^2}}_{FM\ part} + \underbrace{\frac{\left(\Delta f_{FM} / \Delta f_{AM}\right)^2}{1+\left(\Delta f / \Delta f_{AM}\right)^2}}_{AM\ part} \right), \text{ with}$$

$$\Delta f_{AM} = \frac{f_0}{2 \cdot Q \cdot \left| \dfrac{\Delta V / V_0}{\Delta G / G_0} \right|}, \text{ and}$$

$$\Delta f_{FM} = \frac{\pi \cdot F \cdot k \cdot T}{P} \cdot \left(\frac{f_0}{Q}\right)^2 \qquad 3.1$$

where f_0 is the center frequency, Δf is the offset frequency from the carrier, Q is the quality factor of the resonant tank, $\left| \dfrac{\Delta V / V_0}{\Delta G / G_0} \right|$ is the relative dependence of the oscillation amplitude on the load, F is the equivalent noise figure of the active circuit, k is Boltzman's constant, T is the ambient temperature, and P is the power in the resonant tank.

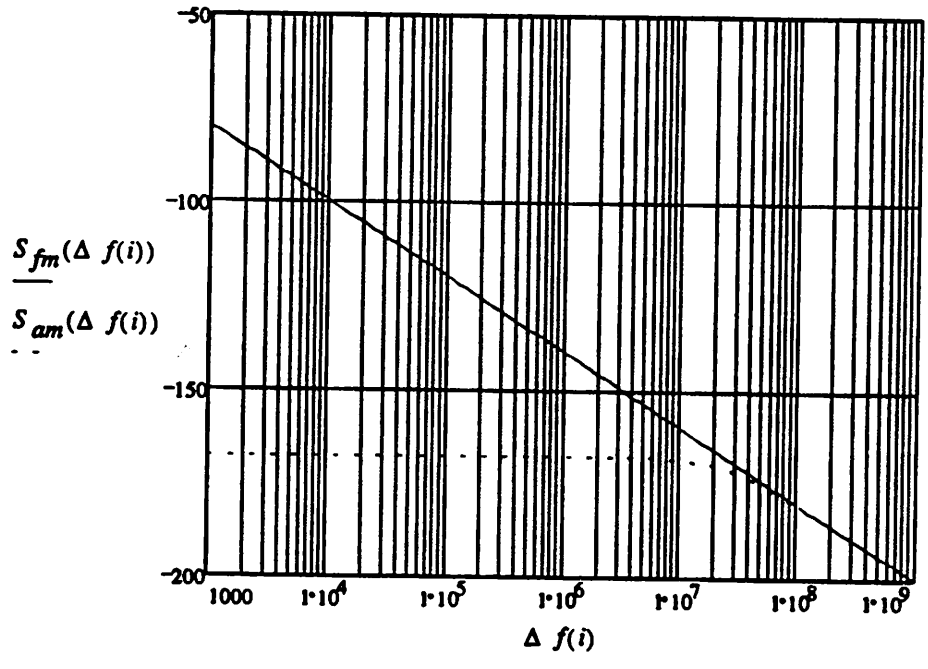

Figure 3.1 AM and FM noise spectral density (dBc/Hz) vs. offset frequency from the carrier (Hz).

The noise spectral density of an oscillator with a center frequency f_0 of 1 GHz, Q of 20, a resonant tank power of 0dBm, and a relative dependence of the oscillation amplitude on the load $\left|\frac{\Delta V/V_0}{\Delta G/G_0}\right|$ of 1 is shown in figure 3.1. It can be seen that at offset frequencies close to the carrier, with $\Delta f < \frac{f_0}{2 \cdot Q}$, spurious phase modulation is dominant; while at larger offset frequencies from the carrier, $\Delta f > \frac{f_0}{2 \cdot Q}$, spurious amplitude modulation has an equal contribution to noise spectral density as spurious phase modulation.

The FM part of (3.1) is equivalently to Leeson's equation [Leeson] for oscillator phase noise. An extension of Leeson's equation to include the effects of flicker noise is given by,

$$\mathcal{L}(\Delta f) = 10 \cdot \log((1 + (\frac{1}{\Delta f} \cdot \frac{f_0}{2 \cdot Q})^2) \cdot (1 + \frac{f_a}{\Delta f}) \cdot \frac{F \cdot k \cdot T}{2 \cdot P}) \text{ in (dBc/Hz)} \qquad 3.2$$

where f_0 is the center frequency, Δf is the offset frequency from the carrier, Q is the quality factor of the resonant tank, f_a is the flicker noise corner frequency, F is the equivalent noise figure of the active circuit, k is Boltzman's constant, T is the ambient temperature, and P is the power in the resonant tank.

3.2 Minimization of Phase Noise

Equations 3.1 and 3.2 can be used as guidelines to minimize the phase noise of an oscillator. The oscillator parameters within control of the designer is the tank Q, the equivalent noise figure of the active circuit F, and the power in the resonant tank P. We can see from equations 3.1 and 3.2 that in order to minimize the phase noise of an oscillator, the design needs to have a high Q tank, a low equivalent noise figure of the active circuit, and higher power in the resonant tank.

For a high Q tank, the tank elements can be chosen appropriately. Having a tank with high Q is equivalent to having a resonant network with a steep phase slope of the impedance for a series resonant tank or a steep phase slope of the admittance for a parallel resonant tank. Consider the circuit in figure 2.3b, repeated here as figure 3.2.

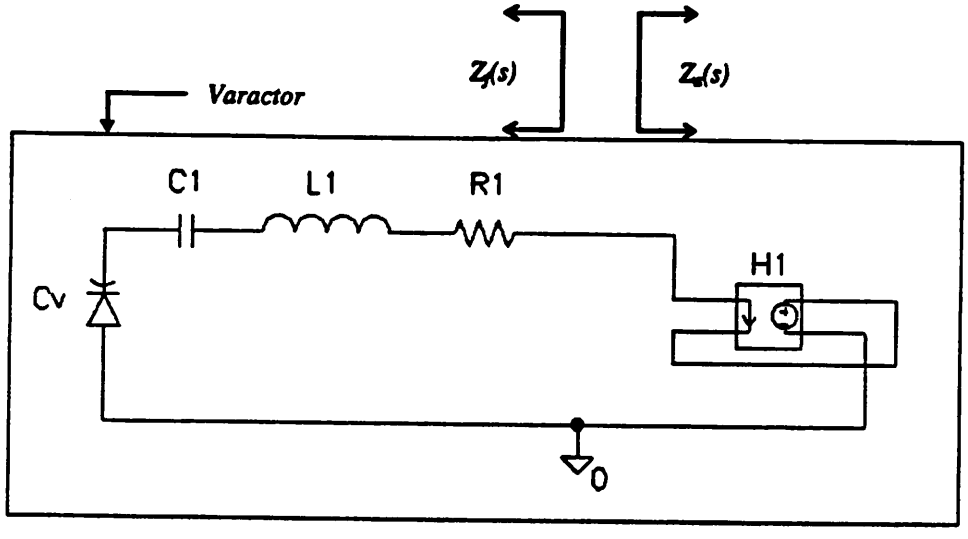

Figure 3.2 ICNR with varactor-tuned series resonant tank.

The impedance of the frequency-determining part is

$$Z_f(\omega) = R + j\cdot(\omega\cdot L - \frac{1}{\omega\cdot C}) \qquad 3.3$$

where $R = R_1$, $L = L_1$, and $C = \frac{1}{\frac{1}{C_1}+\frac{1}{C_V}}$. The phase of the impedance is, then,

$$\theta(\omega) = \tan^{-1}(\frac{\omega\cdot L}{R} - \frac{1}{\omega\cdot R\cdot C}).$$

If we let $Q = \frac{\omega_0\cdot L}{R}$ and $\omega_0^2 = \frac{1}{L\cdot C}$,

$$\theta(\omega) = \tan^{-1}(Q\cdot(\frac{\omega}{\omega_0} - \frac{\omega_0}{\omega})).$$

The slope of the phase of the impedance is, then,

$$\frac{d\theta(\omega)}{d\omega} = \frac{Q}{1+Q^2\cdot(\frac{\omega}{\omega_0}-\frac{\omega_0}{\omega})^2}\cdot(\frac{1}{\omega_0}+\frac{\omega_0}{\omega^2}).$$

However,

$$\left.\frac{d\theta(\omega)}{d\omega}\right|_{\omega=\omega_0} = \frac{2\cdot Q}{\omega_0}. \qquad 3.4$$

Hence, the slope of the phase of the impedance of the frequency-determining circuit is proportional to the Q of resonant tank.

The amount of power delivered into the tank, however, may be limited by power consumption considerations and the available headroom in designs with lower supply voltages. Care also must be taken, in varactor-tuned tank circuits, to ensure that the varactors are not forward-biased by the voltage swing across them, especially under lower back-biased voltages, since the nonlinearities of forward-biased varactors may significantly degrade the performance of the oscillator.

The equivalent noise figure of the oscillator active circuit, on the other hand, can be minimized by proper design. According to [Mullen], a comprehensive description of oscillator noise is possible with the equivalent noise circuit in figure 3.3. The conductance G comprises of all the losses in the oscillator. The active circuit is represented by $i(v)$, a VCNR, and the noise-current generator i_{nG} consists of the thermal noise of the conductance G and the noise contribution of the active circuit.

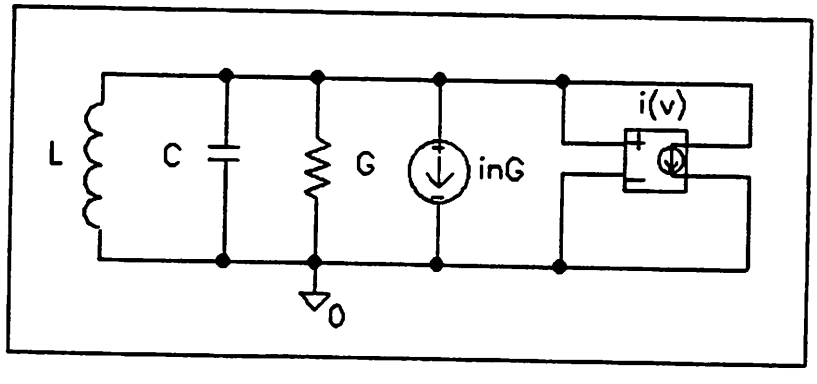

Figure 3.3 Equivalent noise circuit of an oscillator.

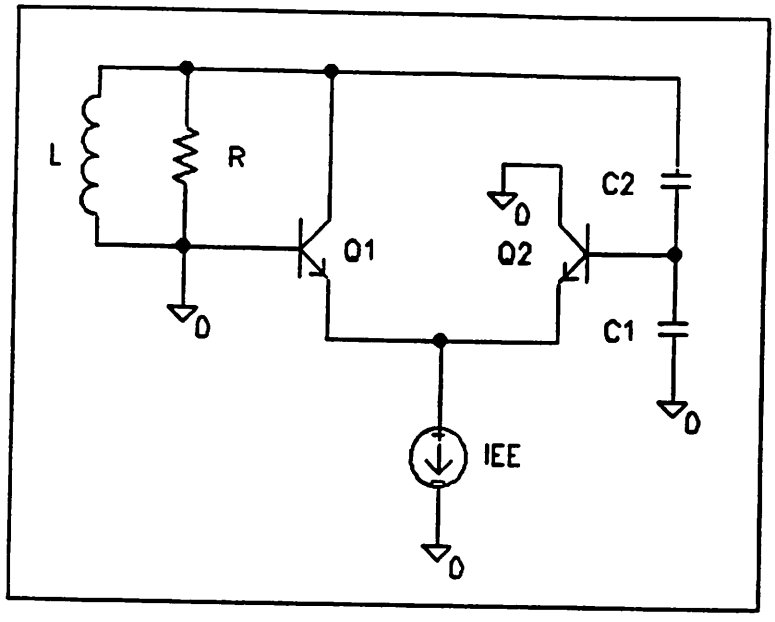

Figure 3.4 Emitter-coupled pair oscillator.

Figure 3.4 presents an emitter-coupled pair oscillator with a parallel resonant tank formed by L and $C=\frac{1}{\frac{1}{C_1}+\frac{1}{C_2}}$. The equivalent noise circuit of this oscillator which contains an idealized active circuit with a forward transconductance g_m is shown in figure 3.5. The noise-current generator i_n and the noise-voltage generator v_n describe the oscillator noise contribution from the active circuit. The effective load resistor R includes all the losses in the resonant circuit resulting in an equivalent noise-current generator i_{nR}. The feedback network, formed by C_1 and C_2, is modeled by a transformer with a voltage step-down ratio $n=1+\frac{C_1}{C_2}$.

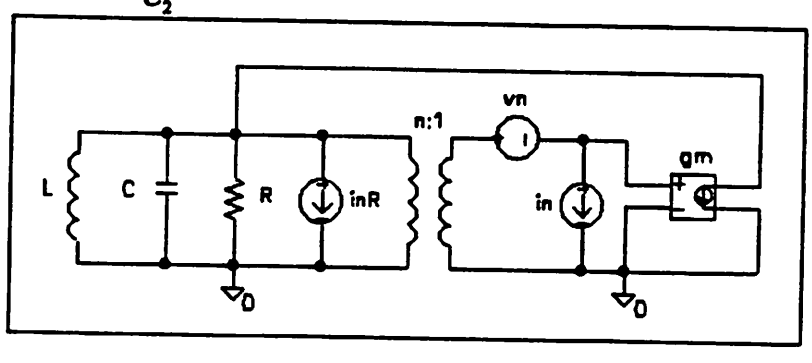

Figure 3.5 Equivalent noise circuit of the emitter-coupled pair oscillator in figure 3.4.

The equivalent noise circuit of figure 3.5 will now be transformed into the simple equivalent noise circuit of figure 3.3, in which all noise generators are combined into one equivalent noise-current generator i_{nG} parallel to the resonant circuit [Lindenmeier]. To do this, the noise of the active circuit has to be transformed into a noise-current generator i_{nT} that is parallel to the resonant circuit. The noise-current generator i_{nR} of the equivalent load resistor R is already situated at the appropriate location. Hence, we have

$$\overline{i_{nG}^2} = \overline{i_{nR}^2} + \overline{i_{nT}^2} \qquad 3.5$$

$$\text{where } \overline{i_{nR}^2} = \frac{4 \cdot k \cdot T \cdot \Delta f}{R} \qquad 3.6$$

$$\text{and } \overline{i_{nT}^2} = \frac{\overline{i_n^2}}{n^2} + g_m^2 \cdot \overline{v_n^2} \qquad 3.7$$

$$\text{with } \overline{i_n^2} \approx 2 \cdot q \cdot I_B \cdot \Delta f \text{, assuming } \frac{I_C}{|\beta(j \cdot \omega)|^2} < I_B, \qquad 3.8$$

$$\overline{v_n^2} = 4 \cdot k \cdot T \cdot (2 \cdot r_b + \frac{1}{2 \cdot g_m}) \cdot \Delta f, \qquad 3.9$$

$I_C = \frac{I_{EE}}{2}$, $g_m = \frac{1}{2} \cdot \frac{I_C}{V_T}$, r_b is the base resistance in the transistors, and $V_T \approx 26mV$.

The noise-current generator i_n and the noise-voltage generator v_n are assume to be uncorrelated. This assumption is valid as long as $\frac{I_C}{|\beta(j \cdot \omega)|^2} < I_B$, i.e. the frequency of operation f_0 is less than $\frac{f_T}{\sqrt{\beta_0}}$.

However, the steady-state operation of the oscillator requires that

$$\frac{g_m}{n} = \frac{1}{R}. \qquad 3.10$$

Equation 3.7 becomes

$$\overline{i_{nT}^2} = \frac{\overline{i_n^2}}{n^2} + \frac{n^2}{R^2} \cdot \overline{v_n^2}. \qquad 3.11$$

The noise figure of the oscillator is then given by [Lindenmeier],

$$F = \frac{\overline{i_{nR}^2} + \overline{i_{nT}^2}}{\overline{i_{nR}^2}} = 1 + \frac{\overline{i_{nT}^2}}{\overline{i_{nR}^2}}$$

$$F = 1 + \frac{1}{4 \cdot k \cdot T \cdot \Delta f} \cdot (\frac{R}{n^2} \cdot \overline{i_n^2} + \frac{n^2}{R} \cdot \overline{v_n^2}). \qquad 3.12$$

From equation 3.12, we can see that the noise figure of an oscillator can be optimized for a given active circuit by choosing an appropriate feedback factor n to perform noise matching analogous to the principle of noise matching in amplifier circuits [Lindenmeier]. The optimum feedback factor n_{opt} can shown to be

$$n_{opt} = \sqrt{\frac{R}{\sqrt{\frac{\overline{v_n^2}}{\overline{i_n^2}}}}}. \qquad 3.13$$

Figure 3.6 shows the noise figure of the ECP oscillator in figure 3.4 with $R = 1k\Omega$ and $I_{EE} = 3mA$ as a function of the feedback factor n for different values of r_b. For large values of n, the noise figure is dominated by the transformed equivalent noise-voltage of the active circuit and, hence, is dependent on the base resistance of the transistors r_b. Whereas for small values of n it is dominated by the transformed equivalent noise-current of the active circuit and is weakly dependent on the base resistance of the transistors r_b. The optimum feedback factor n shifts from $n \approx 2.1$ for $r_b = 0\Omega$ resulting in a noise figure of 0.5dB to $n \approx 1.2$ for $r_b = 50\Omega$ resulting in a noise figure of 1.5dB.

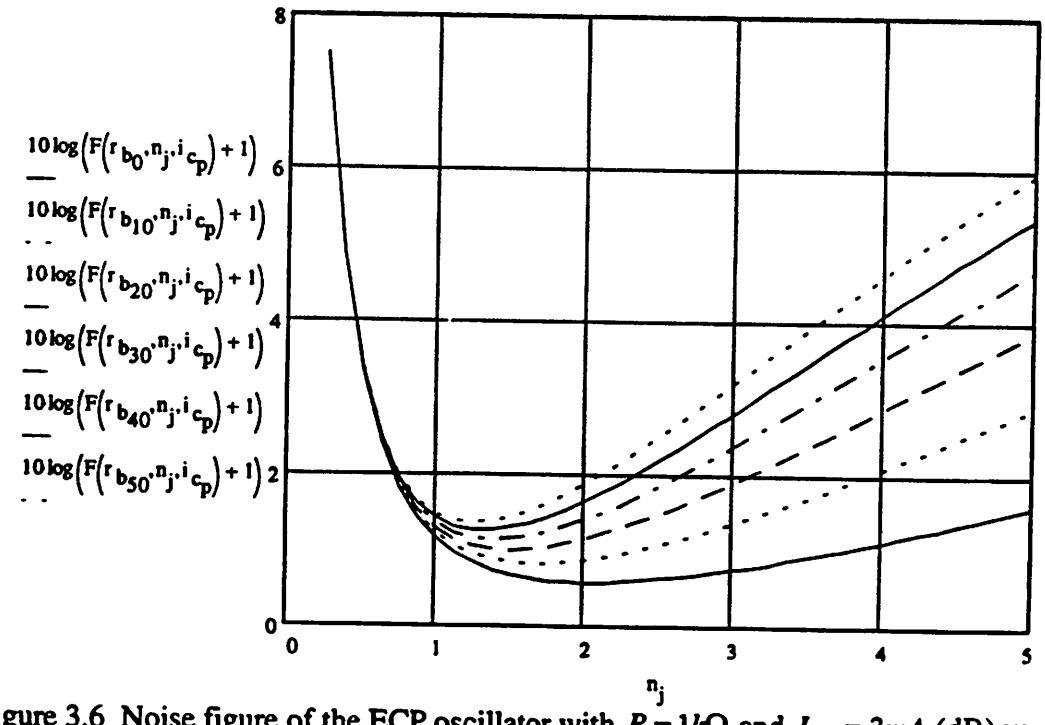

Figure 3.6 Noise figure of the ECP oscillator with $R = 1k\Omega$ and $I_{EE} = 3mA$ (dB) vs. feedback factor n for r_b=0, 10, 20, 30, 40, and 50 ohm.

A contour plot of the noise figure of the oscillator as a function of the feedback factor n and the base resistance of the transistors r_b is shown in figure 3.7. We can see that the sensitivity of the noise figure of the oscillator to the feedback factor n is reduced for smaller base resistances of the transistors.

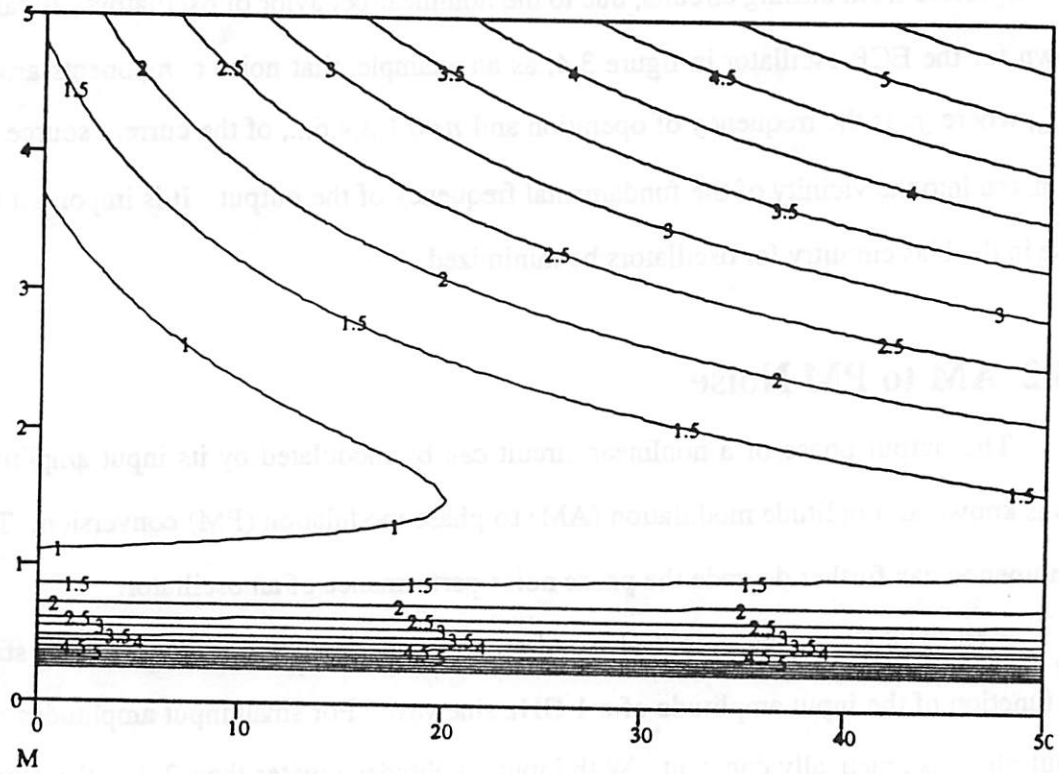

Figure 3.7 Noise figure contours of the ECP oscillator with $R = 1k\Omega$ and $I_{EE} = 3mA$ (dB) vs. feedback factor n (vertical) and base resistance r_b (Ω) (horizontal).

Please note that equation 3.12 gives a first-order approximation for the noise figure of the oscillator since it does not take into account the time-varying nature of the correlation of the noise-current and noise-voltage generators. Other approaches which include time-varying effects of circuits and can lend themselves to numerical computation [Kaertner, Hull] may be used.

3.3 Other Considerations

3.3.1 Bias Circuitry Noise

Noise in oscillators (which would not be present otherwise for linear circuits) can also originated from biasing circuits, due to the nonlinear behavior of oscillators. It can be shown for the ECP oscillator in figure 3.4, as an example, that noise components around $n \cdot f_0$, where f_0 is the frequency of operation and n=0,1,2,4,6..., of the current source I_{EE} are mixed into the vicinity of the fundamental frequency of the output. It is important that noise in the bias circuitry for oscillators be minimized.

3.3.2 AM to PM Noise

The output phase of a nonlinear circuit can be modulated by its input amplitude. This is known as amplitude modulation (AM) to phase modulation (PM) conversion. This phenomenon can further degrade the phase noise performance of an oscillator.

Figure 3.8 shows the output phase of an undegenerated emitter-coupled pair stage as a function of the input amplitude of a 1 GHz sinewave. For small input amplitudes, the output phase is practically constant. With input amplitudes greater than $2 \cdot V_T$, the output phase starts to become dependent on the input amplitude. The change in output phase as a function of the input amplitude (figure 3.9) is the highest for input amplitudes of $2 \cdot V_T$ to $3 \cdot V_T$ and is reduced for larger input amplitudes.

A larger steady state oscillation amplitude ($\approx 10 \cdot V_T$ for an emitter-coupled pair) is not only desirable for having sufficient initial loop gain to ensure reliable start-ups [Meyer] but also for minimizing AM to PM conversion in the active circuit.

Figure 3.8 Output phase of an undegenerated emitter-coupled pair stage (degrees) vs. input amplitude of a 1 GHz sinewave ($V_{0\text{-}peak}$).

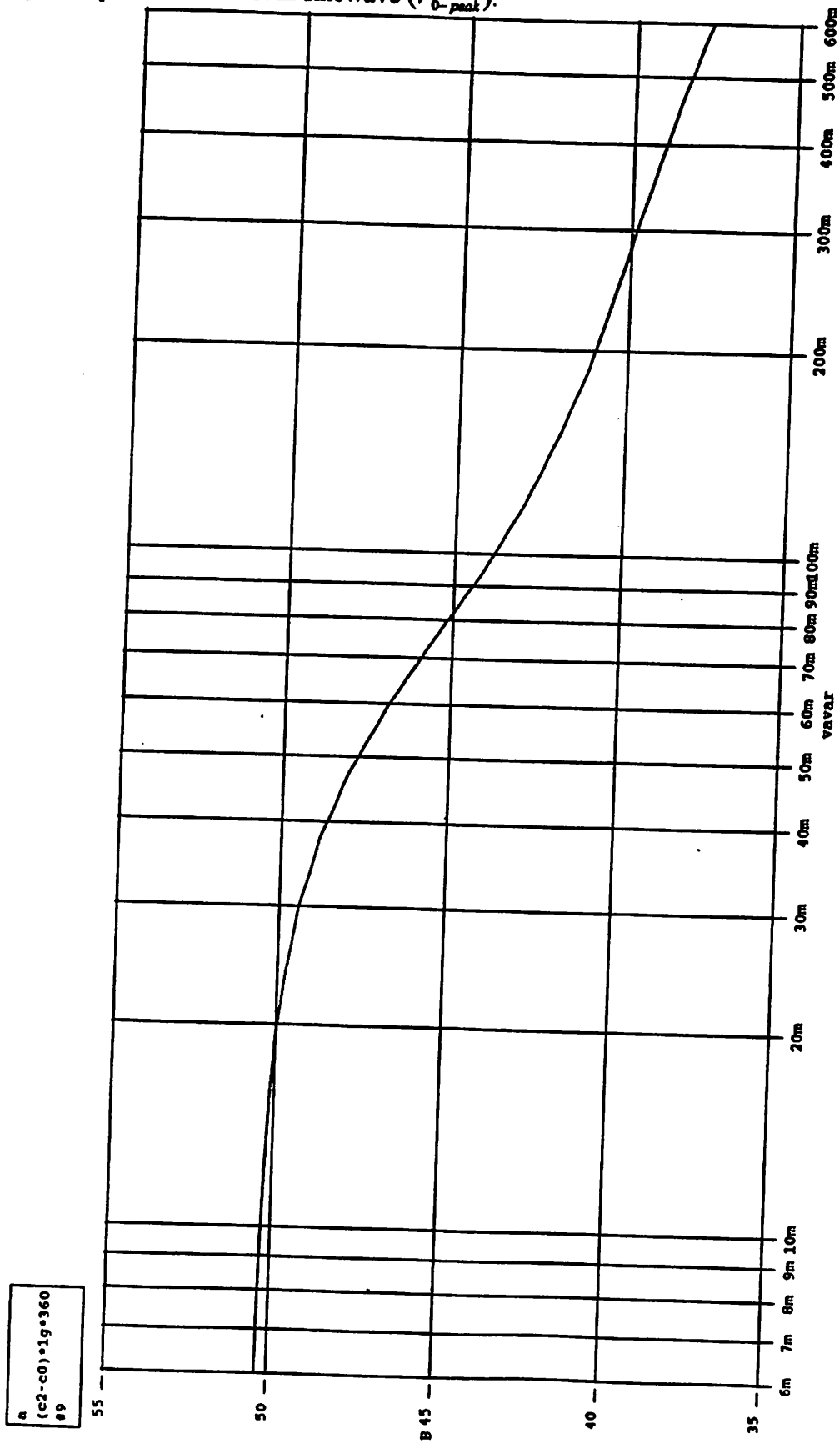

Figure 3.9 Change in output phase of an ECP vs. input amplitude of a 1 GHz sinewave (V_{0-peak}).

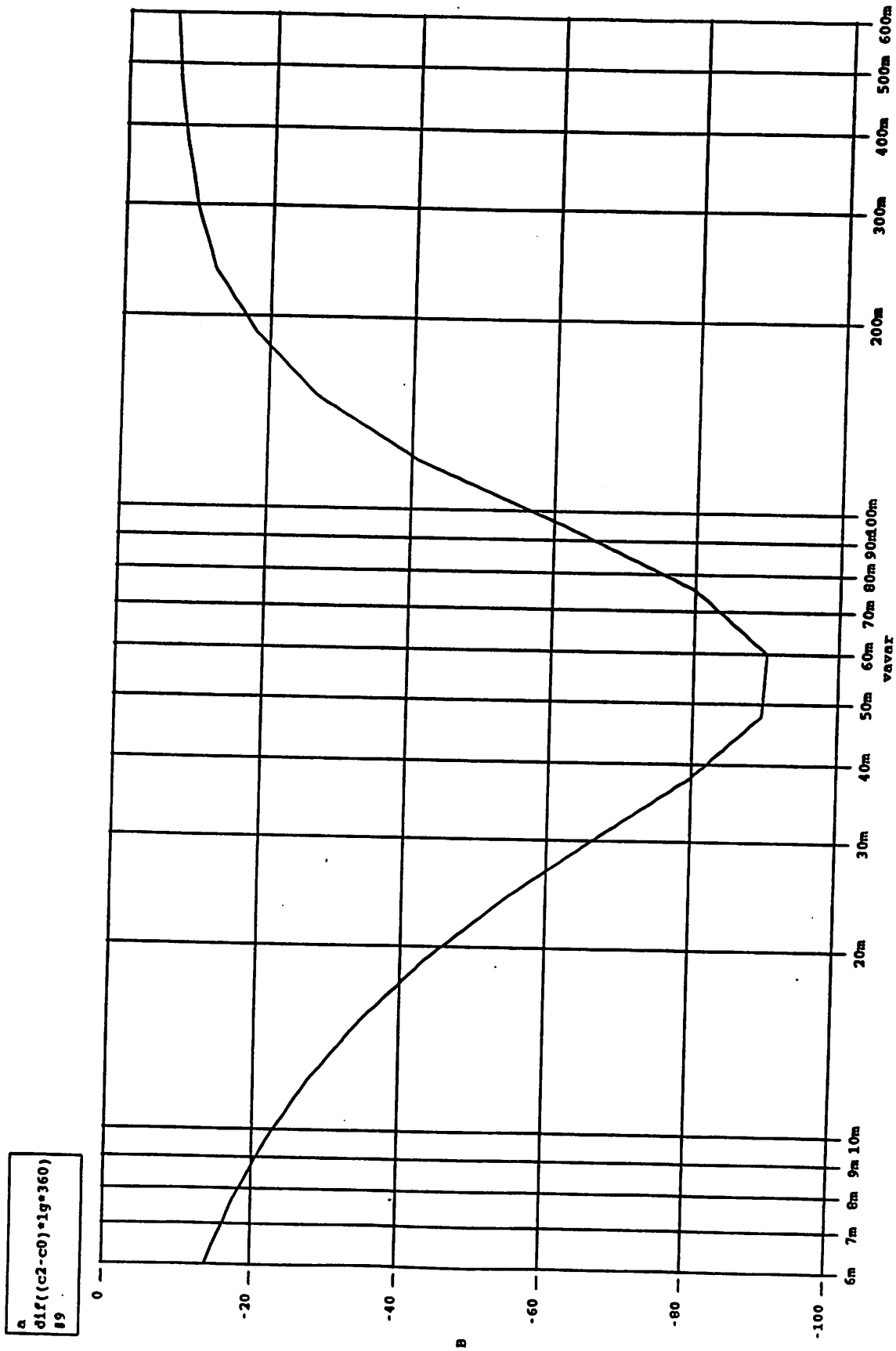

4 A Monolithic RF LC Voltage-Controlled Oscillator

A monolithic fully differential RF LC voltage-controlled oscillator designed using on-chip spiral inductors and varactors and emitter-coupled pair as the active circuit is shown in figure 4.1 (simplified schematic). The VCO is designed to operate over a supply voltage range of 2.7V to 5V.

The fully differential architecture of the VCO provides more power supply rejection as well more common mode radiation immunity compared to single-ended designs. Better radiation immunity of the resonators help minimize the possibility of pulling of the center frequency of the VCO due to the presence of a larger signal near the center frequency.

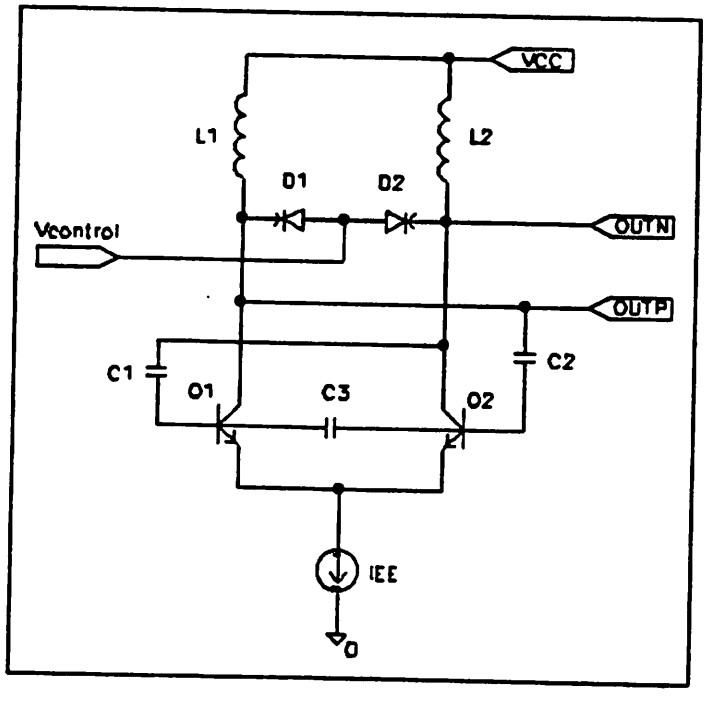

Figure 4.1 Monolithic LC emitter-coupled pair voltage-controlled oscillator.

The tank is formed by the inductors L1 and L2, the varactors D1 and D2, and the differential capacitive feedback network consisting of C1, C2 and C3. The feedback factor of the VCO is $1+\frac{2\cdot C_3}{C_1}$ or $1+\frac{2\cdot C_3}{C_1}$. The Q of the tank is ≈ 3 and this is dominated by the metal resistance losses of the spiral inductors. The emitter-coupled pair formed by Q1 and Q2 is used as the active circuit. The control voltage $V_{control}$ controls the operating frequency of the VCO by changing the amount of reverse voltage of the varactors D_1 and D_2 relative to V_{CC}.

The outputs *outp* and *outn* go to a differential to single-ended buffer which is capable of driving 50Ω impedance off-chip. The buffer also helps provide isolation between the resonant tank and the output load of 50Ω. I_{EE} is set at 4mA, L1=L2, D1=D2, and C1=C2.

The VCO has been fabricated in a process with $f_T \approx 25GHz$. Figure 4.2 shows a plot of the measured output frequency versus control voltage relative to VCC; the VCO has a tuning sensitivity of ~60MHz/V and should provide sufficient tuning range to cover tolerances in the tank even for a limited control voltage range. Figure 4.3 shows the measured output power versus output frequency. We can see that the output power variation over frequency is around 1dB. The slight increase in output power with frequency is due to the increasing Q of the inductors with frequency.

The measured output frequency versus supply voltage is plotted in figure 4.4; while the output power versus supply voltage is plotted in figure 4.4. The variation in output frequency is 2.2 MHz over the supply range of 2.7V to 5V. The output power variation over the supply range is 1dB.

Figure 4.6 shows the output spectrum of the voltage-controlled oscillator. The harmonics of the output are all less than -35dBc. A close-in spectral plot of the carrier is shown in Figure 4.7.

Figure 4.8 shows a plot of the oscillator phase noise. The phase noise is -98dBc/Hz at a 100kHz offset from the carrier frequency of 823MHz.

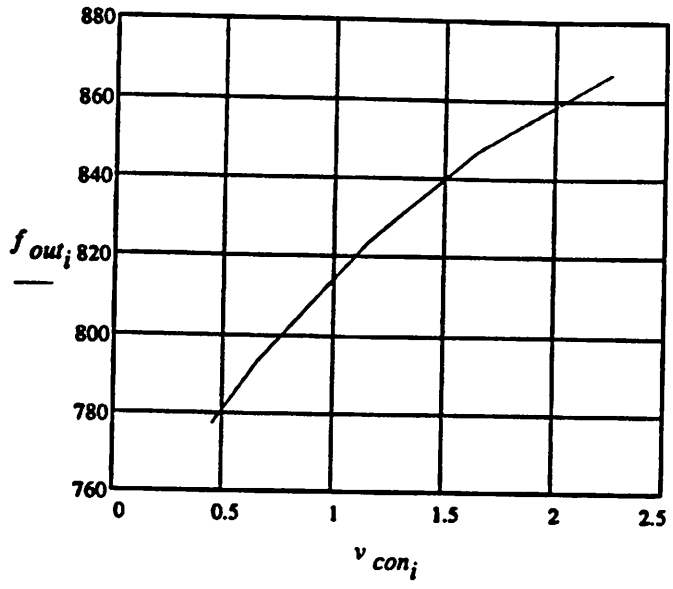

Figure 4.2 Output frequency (MHz) vs. control voltage relative to VCC (V).

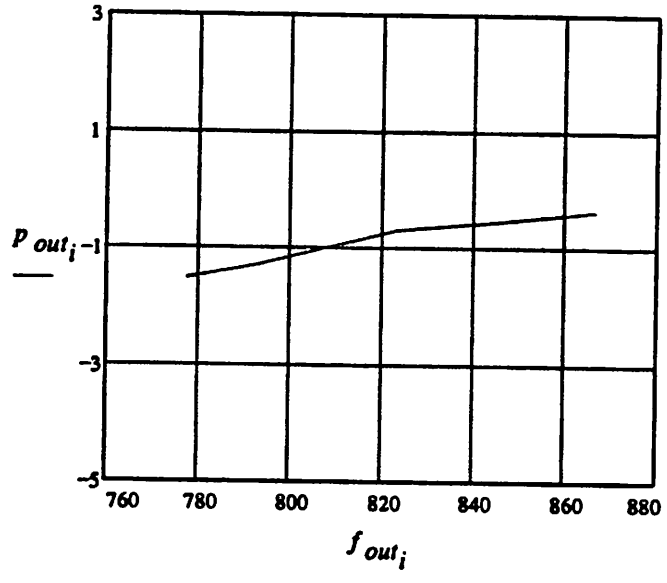

Figure 4.3 Output power (dBm) vs. output frequency (MHz).

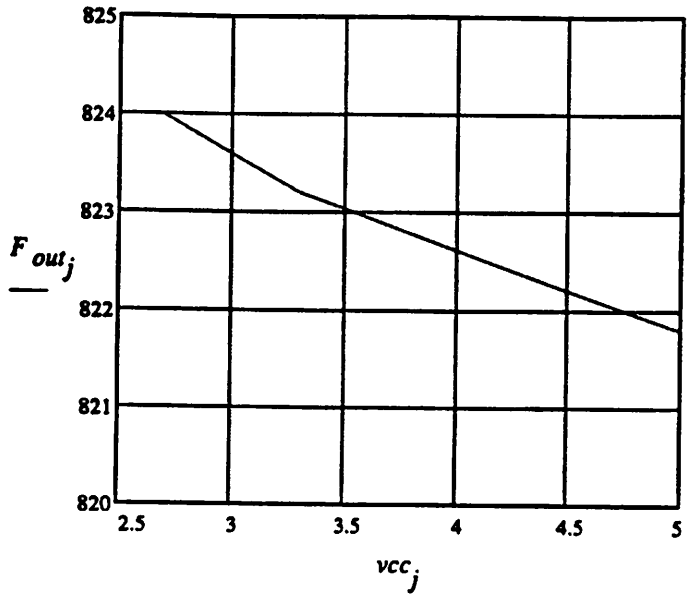

Figure 4.4 Output frequency (MHz) vs. supply voltage (V).

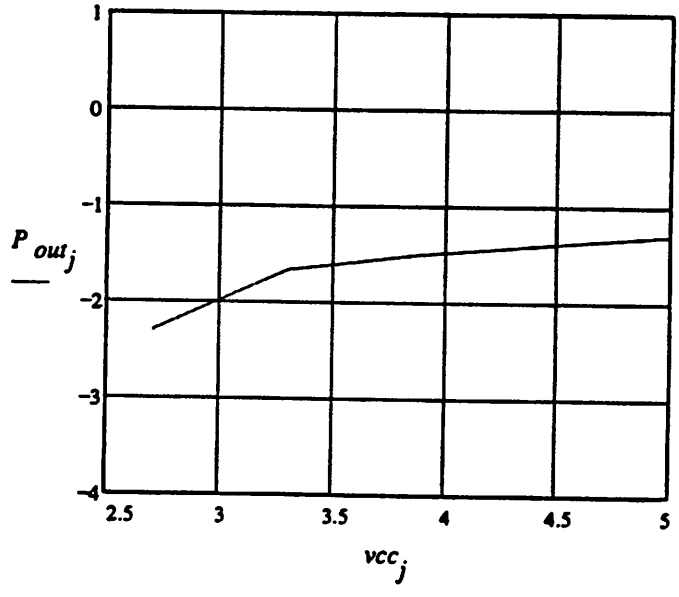

Figure 4.5 Output power (dBm) vs. supply voltage (V).

Figure 4.6 Output spectrum of the voltage-controlled oscillator.

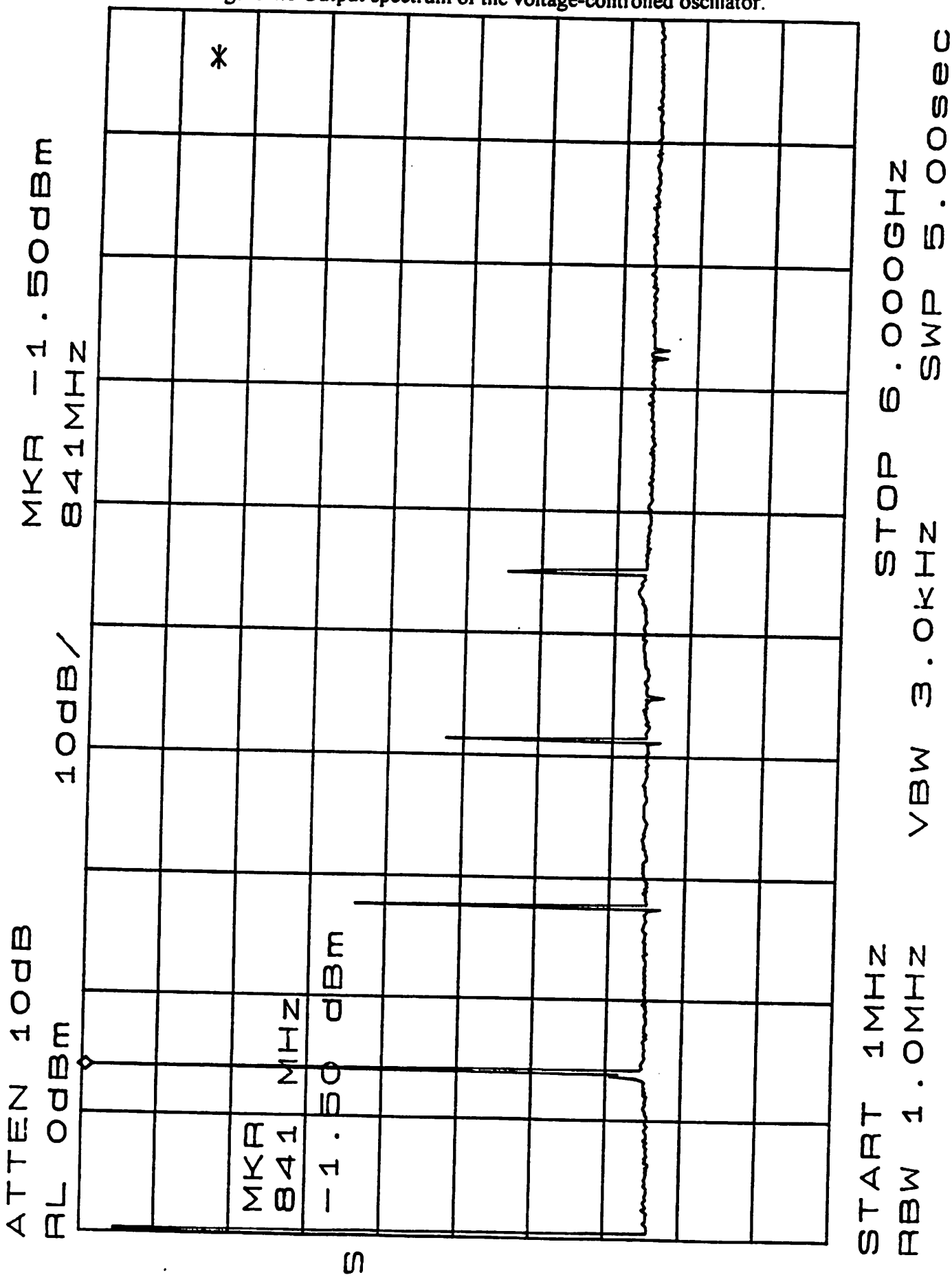

Figure 4.7 Close-in output spectrum of the voltage-controlled oscillator.

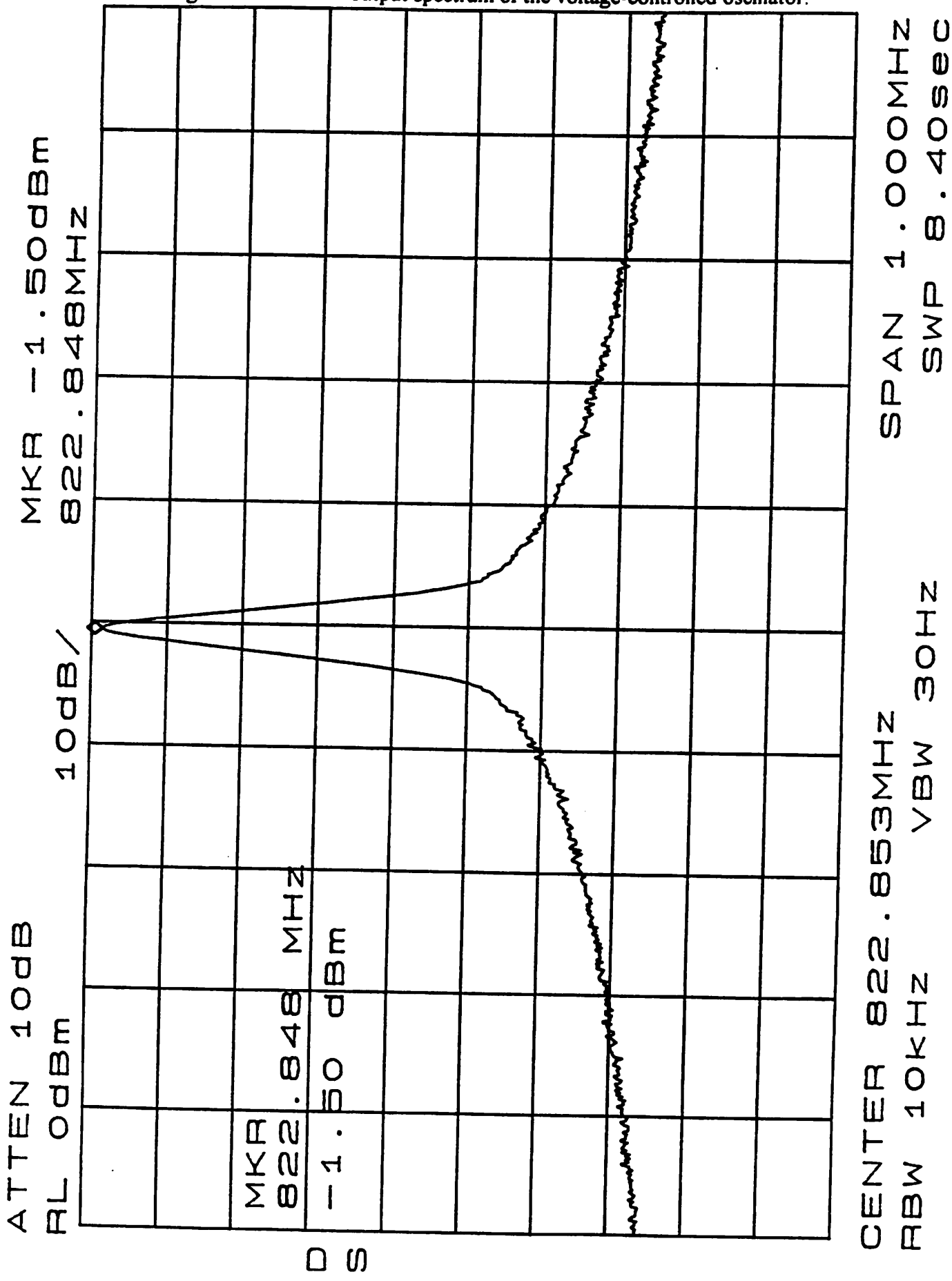

Figure 4.8 Voltage-controlled oscillator phase noise.

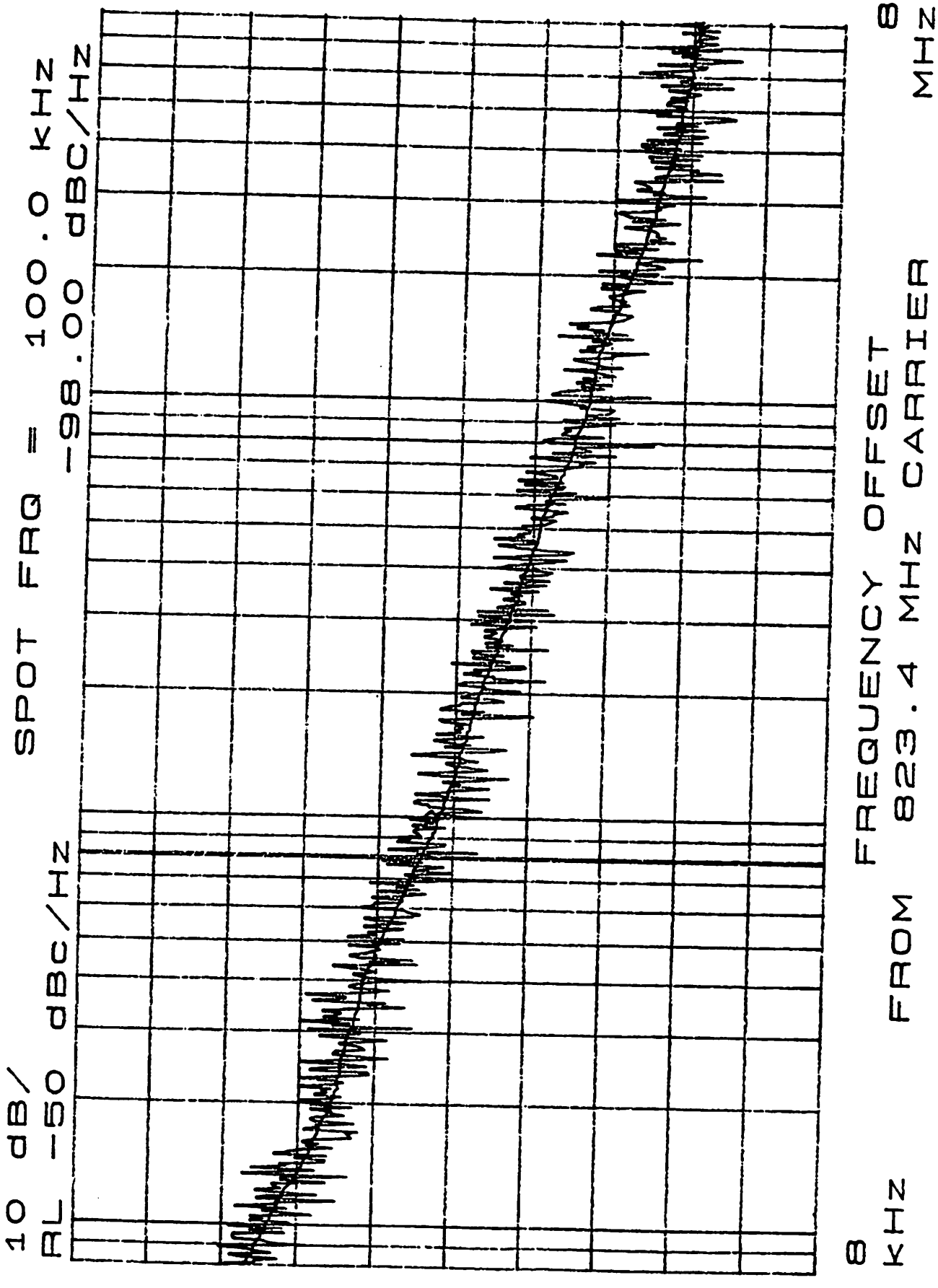

5 Determination of Resonator to Load Isolation with Injection-Locking of Oscillators

Good isolation between resonator and load of oscillators is advantageous to minimize the effects of variation of the load on the operation of the oscillator. It is useful to be able to quantify the amount of resonator to load isolation as a figure of merit for immunity to load variations. In monolithic oscillators, it may be difficult to have access to the resonator nodes without affecting the operation of the oscillators.

A method for determining oscillator resonator to load isolation, using injection locking, without directly accessing the resonator nodes is proposed. Under the appropriate conditions, the application of an external RF signal to the input of an oscillator will cause the oscillator frequency to shift or lock to the frequency of the applied signal, a phenomenon known as injection locking. When the external signal is removed, the oscillator will return to the original mode.

Naturally, an oscillator will not lock to an injected signal of any power or frequency. The locking bandwidth is the frequency range over which an injection-locked oscillator will not break lock. Assuming that the reactive part of the active circuit of the oscillator is independent of oscillation amplitude, the locking bandwidth can be given by [Kurokawa73],

$$B = \frac{2 \cdot \Delta f_i}{f_0} = \frac{2}{Q} \cdot \sqrt{\frac{P_i}{P_r}} \qquad 5.1$$

where B is the locking bandwidth, f_0 is the center frequency of the oscillator, Δf_i is the frequency offset of the injected signal from the center frequency, Q is the quality factor of the resonant tank, P_i is the power of the injected signal at the tank, and P_r is the power in the resonant tank at the center frequency.

We can rewrite 5.1 as

$$B = \frac{2 \cdot \Delta f_i}{f_0} = \frac{2}{Q} \cdot \sqrt{\frac{\alpha \cdot P_i}{P_r}} \qquad 5.2$$

where α is the isolation factor and P_i is now the power of the injected signal at the output of the oscillator.

Consider the setup in figure 5.1. The signal generator is used to inject signals of different power levels and at different frequency offsets from the carrier into the output of the oscillator. The spectrum analyzer is used to determine when the oscillator is injection-locked.

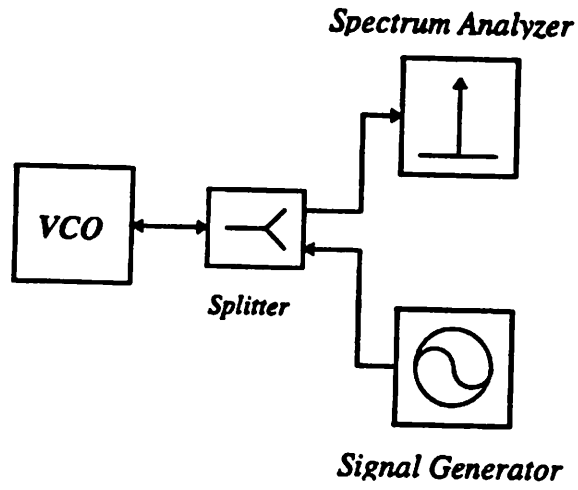

Figure 5.1 Measurement setup for determining oscillator resonator to load isolation.

The locking bandwidths of the VCO in figure 4.1 were determined for different injected power levels (see figure 5.2). A least squares fit on the data with equation 5.2 gives $\alpha \approx$ -55dB.

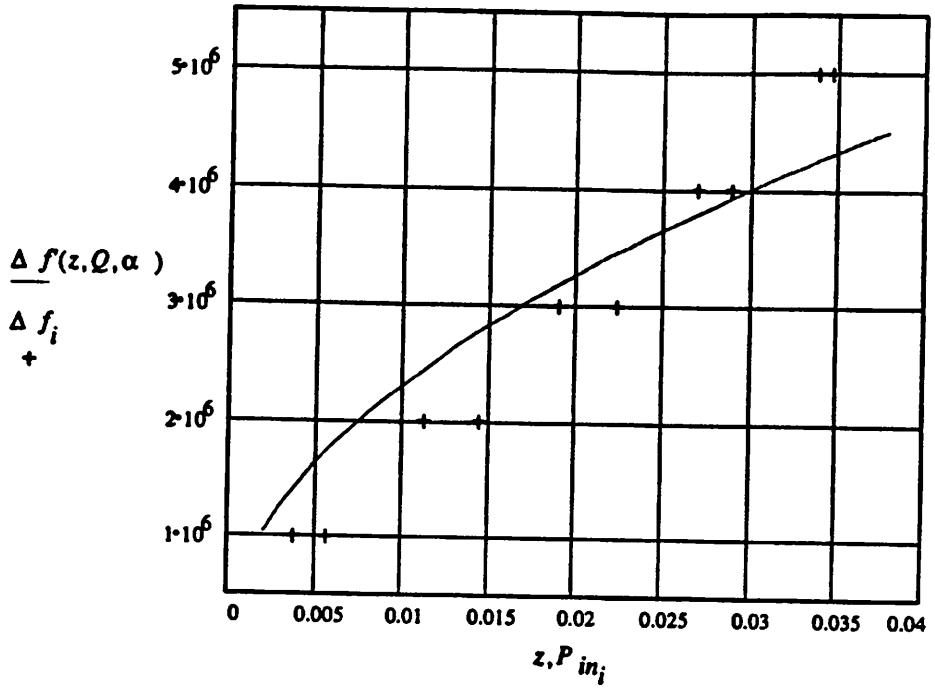

Figure 5.2 Locking bandwidth (Hz) vs. injected power at the output of the oscillator (W).

Figures 5.3 through 5.7 show the output spectrum of the VCO from an unlocked state to a locked state (with different levels of power of an injected signal that is offset 1MHz below the unlocked carrier). At the onset of locking, the oscillator output becomes especially noisy. Under a locked state, the oscillator output assumes the phase noise characteristics of the injected signal.

Figure 5.3 Output spectrum of the VCO with P_i= -∞ dBm (unlocked state).

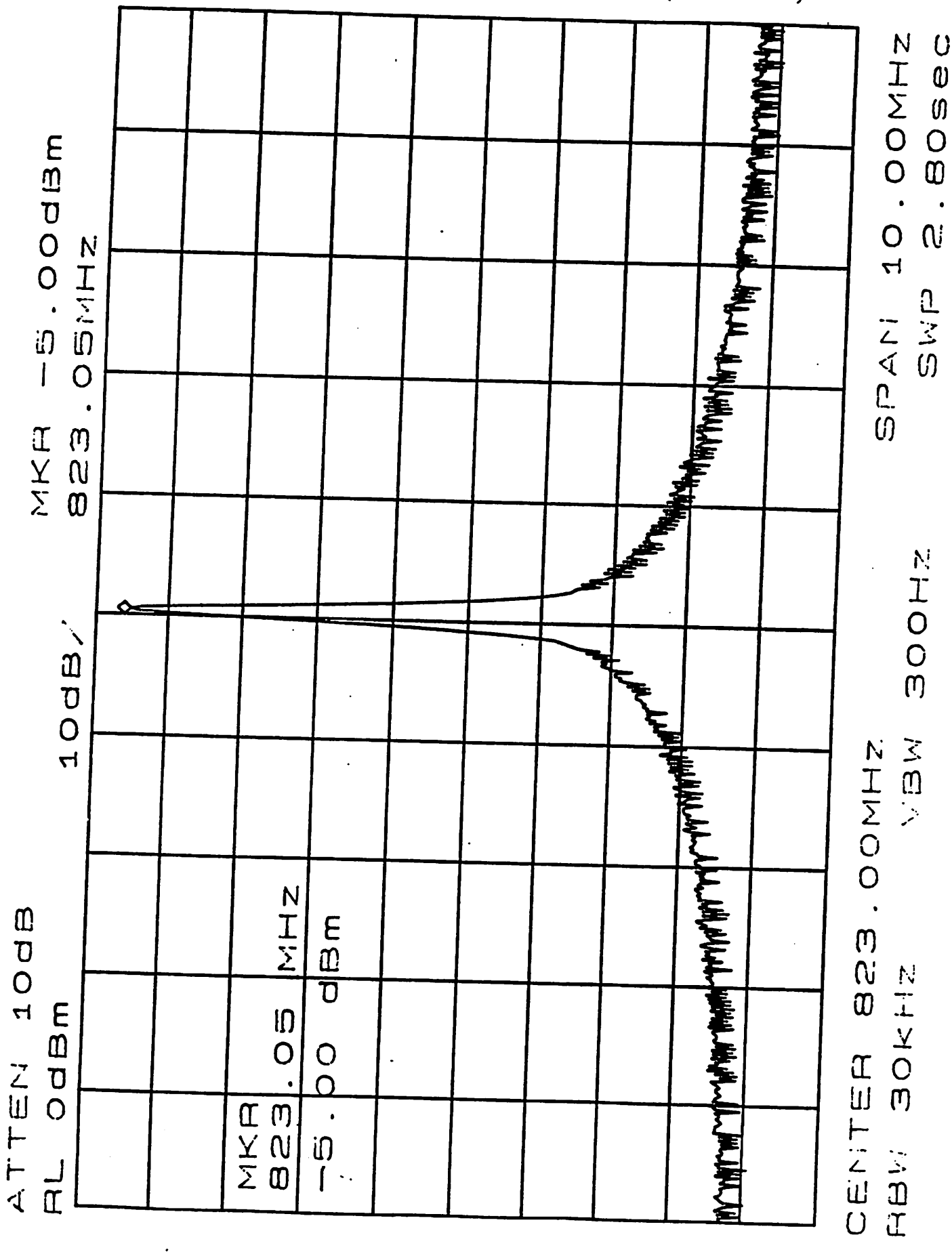

Figure 5.4 Output spectrum of the VCO with P_i= +4.5 dBm (carrier is slightly pulled).

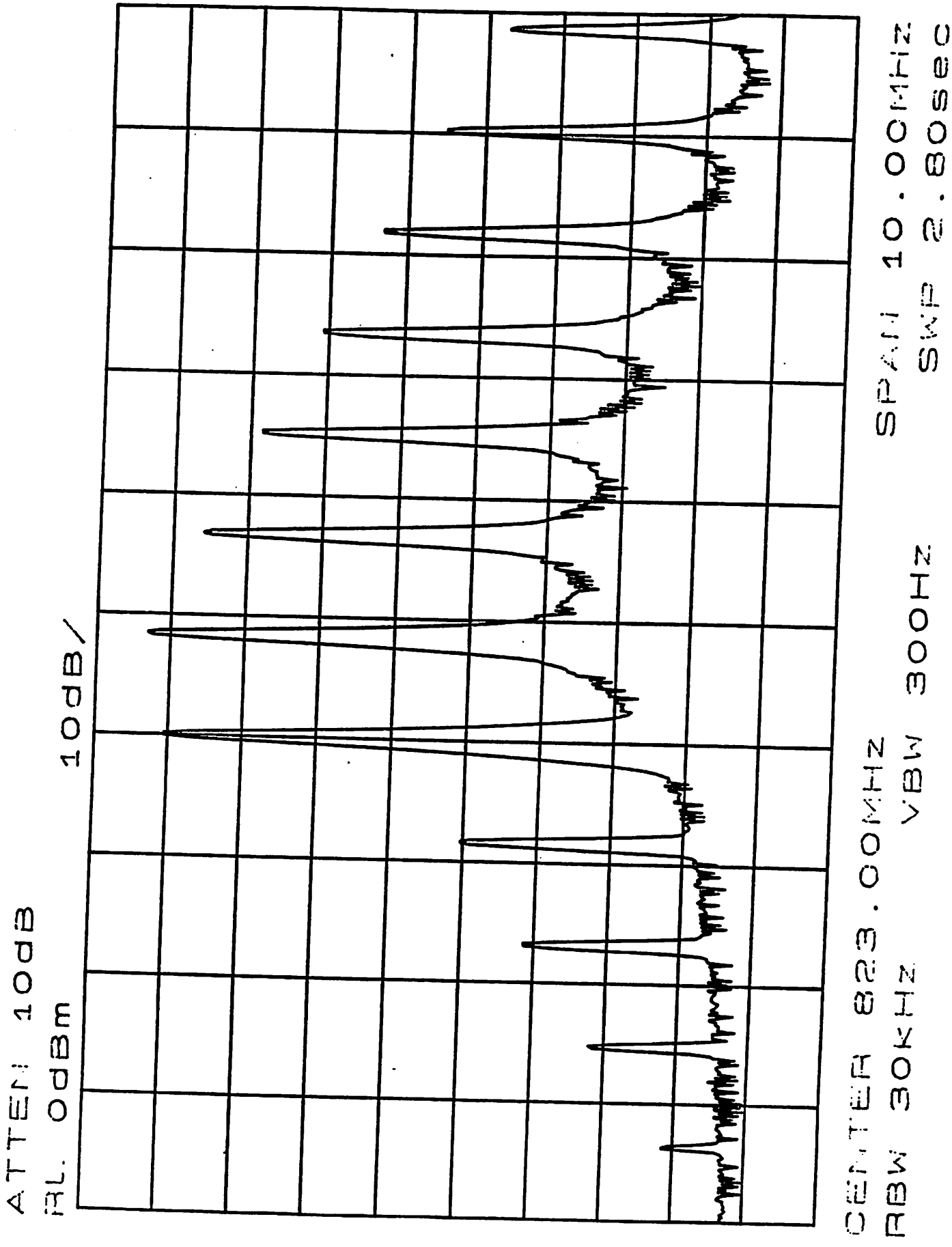

Figure 5.5 Output spectrum of the VCO with P_i= +7.0 dBm (carrier is pulled halfway).

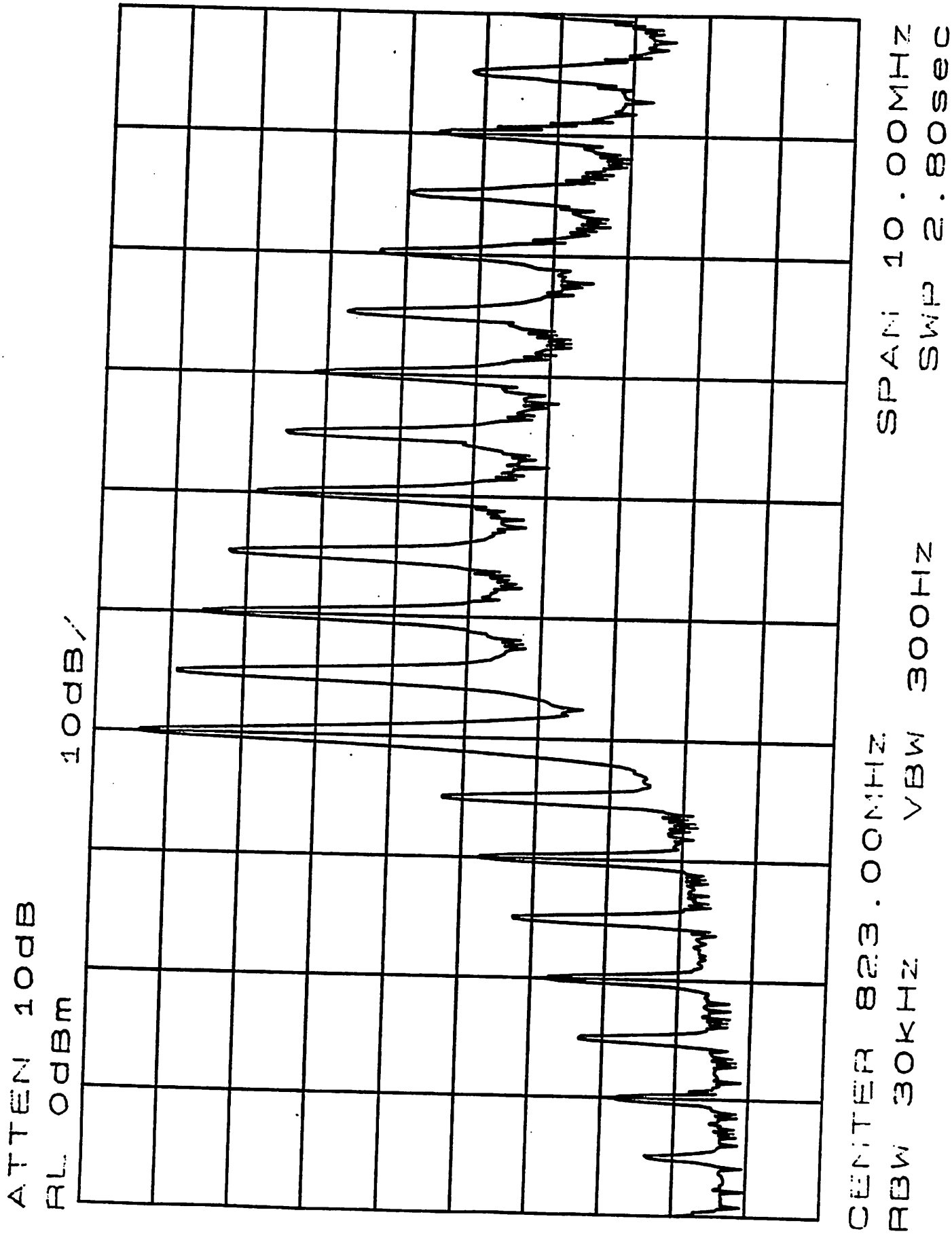

Figure 5.6 Output spectrum of the VCO with P_i= +8.0 dBm (onset of locked state).

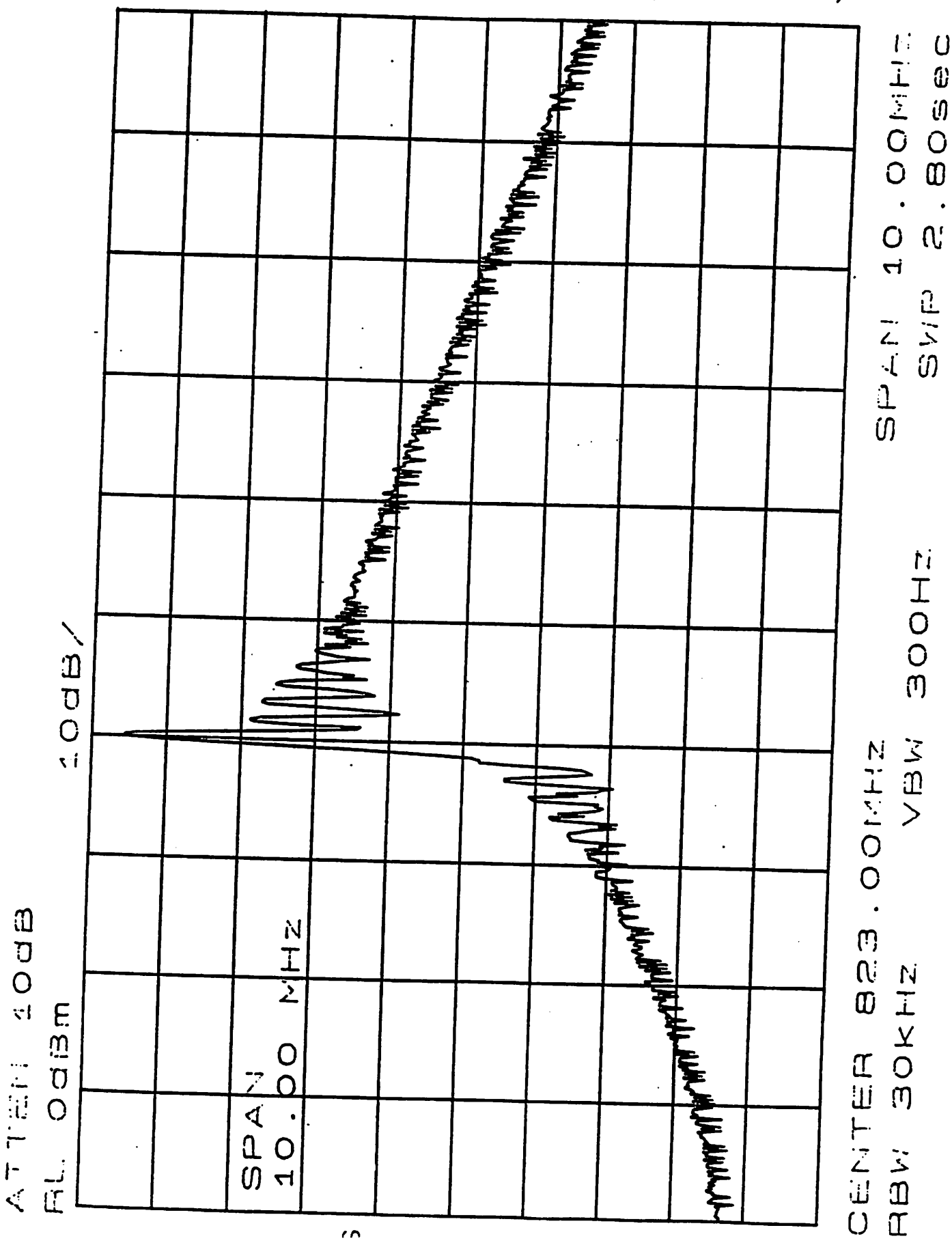

Figure 5.7 Output spectrum of the VCO with P_i= +8.1 dBm (locked state).

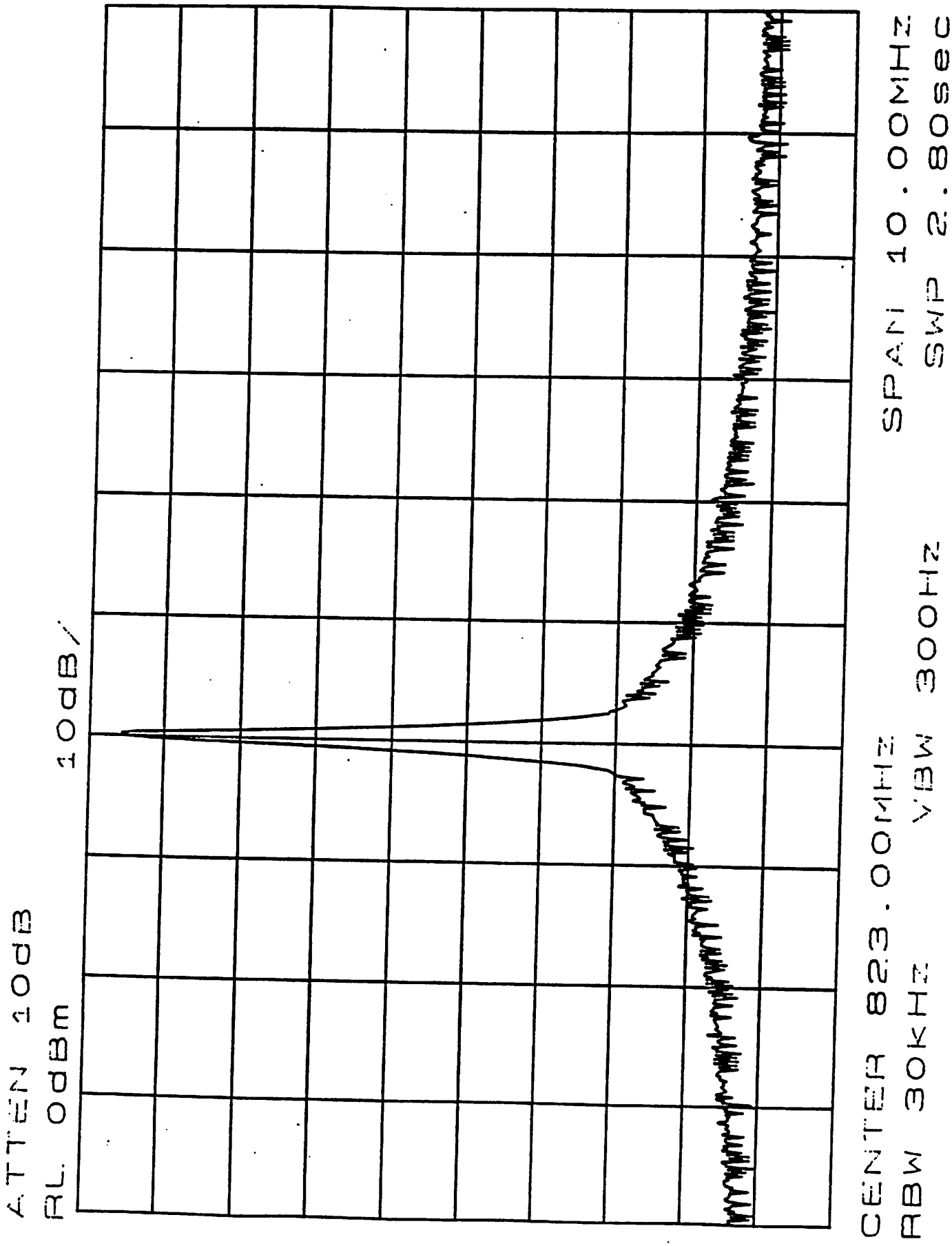

References

[Clarke-Hess] K. K. Clarke and D.T. Hess, *Communication Circuits: Analysis and Design*, Addison Wesley, New York, 1971, Chapter 7.

[Devenport] W. B. Davenport, "Signal-to-Noise Ratios in Band-pass Limiters," *Journal of Applied Physics*, vol. 24, no. 6, pp.720-727, June 1953.

[Gray] P. R. Gray and R.G. Meyer, *Analysis and Design of Analog Integrated Circuits*, Wiley, New York, 1993, Chapter 3.

[Hull] C. D. Hull and R.G. Meyer, "A Systematic Approach to Analysis of Noise in Active Mixers," *IEEE Transactions on Circuits and Systems-I*, vol. 40, no. 12, pp. 909-919, December 1993.

[Kaertner] F. X. Kaertner, "Analysis of White and $f^{-\alpha}$ Noise in Oscillators," *International Journal of Circuit Theory and Applications*, vol. 18, pp. 485-519, 1990.

[Kurokawa68] K. Kurokawa, "Noise in Synchronized Oscillators," *IEEE Transactions on Microwave Theory and Techniques*, vol. MTT-16, no.4, pp. 234-240, April 1968.

[Kurokawa69] K. Kurokawa, "Some Characteristics of Broadband Negative Resistance Oscillator Circuit," *Bell System Technical Journal*, pp. 937-1955, July-August 1969.

[Kurokawa73] K. Kurokawa, "Injection Locking of Microwave Solid-State Oscillators," *Proceedings of the IEEE*, vol. 61, no. 10, pp. 1386-1410, October 1973.

[Leeson] D. B. Leeson, "A Simple Model of Feedback Oscillator Noise Spectrum," *Proceedings of the IEEE*, pp.329-330, February 1966.

[Lindenmeier] H. Lindenmeier, "Noise Matching Techniques in Transistor Oscillators," *Proceedings IEEE Symp. Circuits Syst.* (Houston), pp. 1052-1055, April 1980.

[Maas] S. Maas, *Nonlinear Microwave Circuits*, Artech House, Norwood, 1988, Chapter 12.

[Matyas] R. Matyas, "Effect of Noisy Phase References on Coherent Detection of FFSK Signals," *IEEE Transactions on Communications*, vol. COM-26, no. 6, pp807-815, June 1978.

[Meyer] R. G. Meyer, *Advanced Integrated Circuits for Communication*, EECS 242 Class Notes, University of California, Berkeley, 1992.

[Mullen] J. A. Mullen, "Background Noise in Nonlinear Oscillators," *Proceedings of the IRE*, vol. 8, pp. 1467-1473, 1960.

[Nguyen] N. M. Nguyen and R. G. Meyer, "Start-up and Frequency Stability in High Frequency Oscillators," *IEEE Journal of Solid-State Circuits*, vol. 27, no. 5, pp. 810-820, May 1992.